Paramagnetic States of Four Iron−Four Sulfur Clusters. 1. EPR Single-Crystal Study of 3+ and 1+ Clusters of an Asymmetrical Model Compound and General Model for the Interpretation of the **g**-Tensors of These Two Redox States

Laurent Le Pape,[†] Bernard Lamotte,* Jean-Marie Mouesca, and Gérard Rius[‡]

Contribution from the Département de Recherche Fondamentale sur la Matière Condensée, SCIB/SCPM, C.E.A./Grenoble, 17 rue des Martyrs, 38054 Grenoble Cedex 9, France

Received September 24, 1996. Revised Manuscript Received February 4, 1997[⊗]

Abstract: This article contains (i) an experimental EPR study on $[4Fe-4S]^{3+}$ and $[4Fe-4S]^{+}$ centers in single crystals of a model compound having an asymmetrical cubane-type cluster and (ii) a theoretical model for the interpretation of **g**-tensors of such states found in synthetic compounds and protein active sites. In the first part, an extensive EPR study of a large number of paramagnetic species with $S = {}^1/_2$ in γ-irradiated single crystals of the $(Et_4N)_2[Fe_4S_4(SC_6H_4\text{-}o\text{-}OH)_4]$ compound (a model complex of active sites of [4Fe−4S] proteins) is reported. This compound represents a simple case of asymmetric 4Fe−4S cluster being well characterized in the crystalline solid state: three iron atoms have the usual tetrahedral coordination with four sulfur atoms, while the fourth one has an extra coordination to the oxygen of the phenol group of its thiolate ligand. Thus, with respect to the local symmetry of its cubane cluster, this compound constitutes formally a representative model of asymmetric active sites, here introduced through the extra pentacoordination. The **g**-tensors of the different paramagnetic species created in $(Et_4N)_2[Fe_4S_4(SC_6H_4\text{-}o\text{-}OH)_4]$ single crystals could be deduced from the angular dependences of the EPR lines in three perpendicular planes. Three different $[4Fe-4S]^{3+}$ centers (with $g_{av} > 2.0023$ and relatively axial **g**-tensors) as well as eight $[4Fe-4S]^{+}$ centers (with $g_{av} \leq 2.0023$ and—most often—rhombic **g**-tensors) were identified. These different species exhibit a large variety of principal values. In the second part, a general model is proposed for the interpretation of the principal values and the principal directions of the **g**-tensors of $[4Fe-4S]^{3+}$ and $[4Fe-4S]^{+}$ centers. It is based on simple qualitative arguments, which are, at first, developed for symmetric compounds of C_{2v} electronic structure. This model allows us to rationalize most of our previous results obtained for single crystals of the $(Et_4N)_2[Fe_4S_4(SCH_2\text{-}Ph)_4]$ compound as well as most of those presented here. This explains the relation existing between the location of the mixed-valence pair in the cubane cluster and the principal direction $\mathbf{V}_1$ corresponding to the largest principal value, g_1, of the **g**-tensor. It is also shown that the two other eigenvalues of the **g**-tensor, g_2 and g_3, are expected to have their corresponding principal directions $\mathbf{V}_2$ and $\mathbf{V}_3$ aligned with the two pairs of identical iron ions. Moreover, in the $[4Fe-4S]^{+}$ state, the existence of two nearly degenerate orbital configurations, called OC1 and OC2, has to be taken into account. Thereafter follows a qualitative discussion of the effects on the **g**-tensors, in the different cases, produced by the introduction of some asymmetry. Finally, this analysis allows us to understand the reasons leading to the number and the diversity of paramagnetic centers observed here and to propose a plausible set of localizations for almost all of them. It also confirms, for the case of the $[4Fe-4S]^{3+}$ states, that taking into account the principal direction $\mathbf{V}_1$ is a valuable tool, a useful "rule of thumb" for the determination of the position of the mixed-valence pair, despite the fact that we deal here with asymmetric compounds. This conclusion is to be contrasted to what can be deduced for the $[4Fe-4S]^{+}$ states because of the greater sensitivity of the ferrous ions, the main source of *g*-anisotropy, to their immediate surrounding. In this last case, we think that such a correlation still makes good sense for a (nearly) symmetric arrangement in which the two ferrous ions are (nearly) equivalent. However, breaking significantly this mirror-type symmetry within the ferrous pair can lead to unpredictable **g**-tensor axes.

Introduction

In most of the iron−sulfur proteins containing [4Fe−4S] active sites already identified and studied, the coordination around each iron atom is close to tetrahedral and involves four sulfur atoms, i.e., three inorganic ones which are part of the cubane cluster itself and one belonging to a cysteine amino acid. However, interest has focused recently on those iron−sulfur proteins with one unique iron atom having coordination different than the three others. Such is the case of the ferredoxin III from *Desulfovibrio africanus*[1,2] and of the ferredoxin of *Pyrococcus furiosus*,[3] both exhibiting an iron atom bound to an aspartic acid instead of a cysteine. But the prototypical, and presently mostly studied, case is that of aconitase, for which Beinert et al. have shown that the single iron ion involved in the catalytic conversion of citrate into isocitrate is bound to H_2O/OH^- in its resting state and to oxygen atoms of the substrate in its active state.[4] Their studies on this protein by Mössbauer, as well as previous work performed with ^{57}Fe ENDOR techniques,[5] have shown that the existence of this distinct

[†] Presently at C.E.A./Grenoble, DRFMC/SCIB, laboratoire de Chimie de Coordination, Unité de Recherche Associée au CNRS No. 1194, 17 rue des Martyrs, 38054 Grenoble Cedex 9, France.

[‡] Presently at the Université de la Rochelle, Pôle Science et Technologie/LEMMA, Avenue Marillac, 17042 La Rochelle, France.

[⊗] Abstract published in *Advance ACS Abstracts,* September 15, 1997.

(1) Armstrong, F. A.; George, S. J.; Cammack, R.; Hatchikian, E. C.; Thomson, A. J. *Biochem. J.* **1989**, *264*, 265.

(2) George, S. J.; Armstrong, F. A.; Hatchikian, E. C.; Thomson, A. J. *Biochem. J.* **1989**, *264*, 275.

(3) Conover, R. C.; Kowal, A. T.; Fu, W.; Park, J.-B.; Aono, S.; Adams, M. W. W.; Johnson, M. K. *J. Biol. Chem.* **1990**, *265*, 8533.

(4) Werst, M. M.; Kennedy, M. C.; Houseman, A. L. P.; Beinert, H.; Hoffman, B. M. *Biochemistry* **1990**, *29*, 10533.

(5) Beinert, H.; Kennedy, M. C. *Eur. J. Biochem.* **1989**, *186*, 5.

S0002-7863(96)03349-5 CCC: $14.00

coordination at one of the iron sites leads to a large asymmetry in the electronic structure and magnetic properties of the cubane as a whole.

The electronic structure and magnetic properties of the paramagnetic states of the iron−sulfur cubanes can be studied in great detail by EPR and ENDOR applied to single crystals of synthetic model compounds.[6−11] The strength of this approach lies in the possibility of obtaining complete **g**-tensors and hyperfine tensors, thus allowing us to characterize in detail paramagnetic $[4Fe-4S]^{3+}$ and $[4Fe-4S]^{+}$ centers. As is well-known by now, the [4Fe−4S] cubanes can appear in three different mixed-valence redox states. Low-potential ferredoxins, and a number of other iron−sulfur proteins, have their oxidized and reduced states corresponding respectively to the $[4Fe-4S]^{2+}$ and $[4Fe-4S]^{+}$ states, while the so-called high-potential iron−sulfur proteins (HiPIP) have their oxidized and reduced states corresponding to the $[4Fe-4S]^{3+}$ and $[4Fe-4S]^{2+}$ states. As far as magnetic properties are concerned, the $[4Fe-4S]^{2+}$ ground state is diamagnetic, while the two $[4Fe-4S]^{+}$ and $[4Fe-4S]^{3+}$ states are paramagnetic and amenable to EPR and ENDOR studies.

The method used in our laboratory relies on the γ-irradiation of single crystals of model compounds in the $[4Fe-4S]^{2+}$ state. Irradiation creates simultaneously, in situ, both the "oxidized" $[4Fe-4S]^{3+}$ and the "reduced" $[4Fe-4S]^{+}$ species. These are trapped at low concentration in the diamagnetic crystalline matrix.[6] The feasibility of this method has been first demonstrated by EPR in single crystals of the $(Bu_4N)_2[Fe_4S_4(SPh)_4]$ synthetic model compound.[7] This work has been then followed by further studies by EPR[10,11] and ENDOR on a $[4Fe-4S]^{3+}$ state in the model compound $(Et_4N)_2[Fe_4S_4(SCH_2Ph)_4]$.[8,9]

The purpose of this article is to present an extensive description, gained from EPR measurements, of the different $[4Fe-4S]^{3+}$ and $[4Fe-4S]^{+}$ paramagnetic species appearing after γ-irradiation in single crystals of the $(Et_4N)_2[Fe_4S_4(SC_6H_4$-*o*-$OH)_4]$ compound. Their analysis will be based on a general theoretical model also developed here concerning the correlation between the **g**-tensor orientation and the mixed-valence pair location. The following companion paper will be devoted to the proton ENDOR study of one of the main $[4Fe-4S]^{+}$ species described here.

As said above, the previous single-crystal EPR and ENDOR studies on paramagnetic states of iron−sulfur cubanes have been initiated in our laboratory on the $(Bu_4N)_2[Fe_4S_4(SPh)_4]$ and $(Et_4N)_2[Fe_4S_4(SCH_2Ph)_4]$ compounds. In those cases, the local environments of the four iron atoms are nearly equivalent. Moreover, the four Fe−S−C ligand bond directions are nearly related by an S_4 symmetry axis around the cubane center. At that stage, ^{57}Fe[8] and proton[9] ENDOR studies on a $[4Fe-4S]^{3+}$ center (called "center IV") in crystals of $(Et_4N)_2[Fe_4S_4(SCH_2$-$Ph)_4]$ showed the following:

(i) The oxidized center could be described as made of two distinct pairs of iron atoms: a delocalized mixed-valence pair $Fe^{2.5+}-Fe^{2.5+}$ and a ferric pair $Fe^{3+}-Fe^{3+}$.

(ii) Within each pair the spin populations on the two iron atoms are nearly equivalent, that is, the electronic structure of this state has a near C_2 axis of symmetry defined by the common perpendicular to the $Fe^{2.5+}-Fe^{2.5+}$ and $Fe^{3+}-Fe^{3+}$ directions.

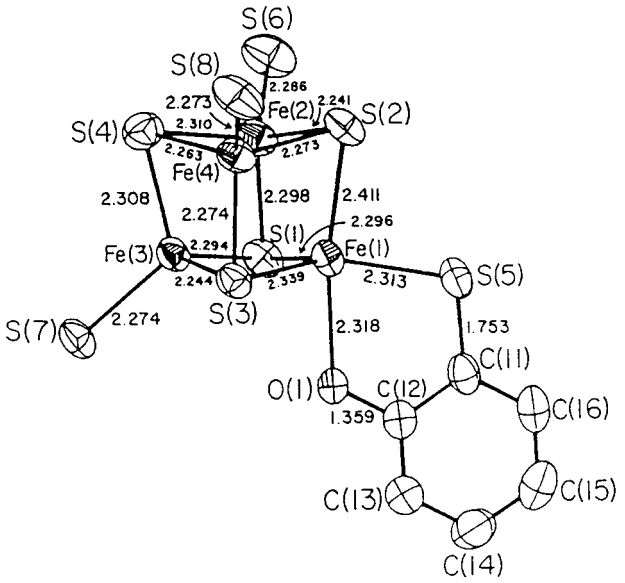

Figure 1. Representation, taken from the X-ray study,[13] of the central part of the $(Et_4N)_2[Fe_4S_4(SC_6H_4$-*o*-$OH)_4]$ core, with the fifth coordination on Fe_1 due to the OH group of the thiolate anion ligand.

Similar conclusions were also arrived at concerning the symmetry of the $[4Fe-4S]^{+}$ centers studied in the same crystals,[12] centers containing a delocalized mixed-valence pair $Fe^{2.5+}-Fe^{2.5+}$ and a ferrous pair $Fe^{2+}-Fe^{2+}$.

In connection with the recent interest in iron−sulfur clusters with one unique coordination site, we have chosen to perform very detailed studies of the paramagnetic states of [4Fe−4S] clusters in single crystals of $(Et_4N)_2[Fe_4S_4(SC_6H_4$-*o*-$OH)_4]$ because this compound represents a simple case of a model system exhibiting an asymmetric ligand coordination in the solid crystalline state. This has been displayed by Johnson et al.,[13] who obtained the corresponding crystallographic structure and showed that, while the Fe_2, Fe_3, and Fe_4 atoms (in their notations) have the normal tetrahedral coordination with their respective thiolate ligand, Fe_1 has an additional fifth coordination with the oxygen of the phenol group belonging to its thiolate ligand, as can be seen in Figure 1. The distances reported in this figure indicate that the oxygen of the ligand, giving rise to the fifth coordination with Fe_1, lies at 2.32 Å, a distance which is comparable to that of Fe_1 to the sulfur of the same thiolate. The cubane geometry is also somewhat distorted: for example, the $Fe_1-S^*_2$ bond length (2.41 Å) is significantly larger (whereas the $Fe_2-S^*_2$ or $Fe_3-S^*_3$ bonds are somewhat smaller: ∼2.24 Å) than the average of the other Fe−S* bond lengths, around 2.30 Å. The same remark is true for the Fe_1-Fe_2 and Fe_1-Fe_4 distances, greater than the others. Moreover, these authors have also reported the Mössbauer spectrum of this compound[13] which indicates that one iron atom exhibits a large quadrupolar interaction $\Delta E_Q = 1.84$ mm·s^{-1} and isomeric shift $\delta = 0.63$ mm·s^{-1}. The other iron atoms are fairly different ($\Delta E_Q = 1.22$ mm·s^{-1}, $\delta = 0.48$ mm.s^{-1} for two equivalent iron atoms and $\Delta E_Q = 0.75$ mm·s^{-1}, $\delta = 0.43$ mm·s^{-1} for the last iron atom). The addition of an extra coordination resulting usually in an increase of the isomer shift, the measured value of 0.63 mm·s^{-1}, corresponds therefore in all likelihood to Fe_1.[13]

As must be now pointed out, the choice of this particular compound was not aimed at mimicing exactly the active site of some particular protein. We treat rather here a well-defined

(6) Gloux, J.; Gloux, P.; Lamotte, B.; Rius, G. *Phys. Rev. Lett.* **1985**, *54*, 599.
(7) Gloux, J.; Gloux, P.; Hendriks, H.; Rius, G. *J. Am. Chem. Soc.* **1987**, *109*, 3220.
(8) Rius, G.; Lamotte, B. *J. Am. Chem. Soc.* **1989**, *111*, 2464.
(9) Mouesca, J.-M.; Rius, G.; Lamotte, B. *J. Am. Chem. Soc.* **1993**, *115*, 4714.
(10) Gloux, J.; Gloux, P.; Lamotte, B.; Mouesca, J.-M.; Rius, G. *J. Am. Chem. Soc.* **1994**, *116*, 1953.
(11) Gloux, J.; Gloux, P. *J. Am. Chem. Soc.* **1995**, *117*, 7513.
(12) Noodleman, L.; Chen, J. L.; Case, D. A.; Giori, C.; Rius, G.; Mouesca, J.-M.; Lamotte, B. In *Nuclear Magnetic Resonance of Paramagnetic Macromolecules*; La Mar, G. N., Ed.; Kluwer Academic Publishers: The Netherlands, 1995; pp 339−367.
(13) Johnson, R. E.; Papaefthymiou, G. C.; Frankel, R. B.; Holm, R. H. *J. Am. Chem. Soc.* **1983**, *105*, 7280.

and representative case of an asymmetric cubane on which we have been able to apply our methods of investigation. We can therefore examine the consequential effects of this asymmetry on the spectroscopic EPR parameters relative to the $[4Fe-4S]^{+}$ and $[4Fe-4S]^{3+}$ centers, i.e., their **g**-tensors.

Experimental Section

(1) Preparation of the $(Et_4N)_2[Fe_4S_4(SC_6H_4$-*o*-$OH)_4]$ Compound and of the Crystal Samples. $(Et_4N)_2[Fe_4S_4(SC_6H_4$-*o*-$OH)_4]$ (**1**) was prepared in two steps. The first step consists in the preparation, by the classical method of Christou and Garner,[14] of $(Et_4N)_2[Fe_4S_4(S$-*t*-$Bu)_4]$ (**2**) from $FeCl_2{\cdot}4H_2O$ (99.999% pure iron). Compound **1** was obtained from compound **2** by ligand exchange with the 2-mercaptophenol (HSC_6H_4-*o*-OH) in acetonitrile solution. Single crystals of **1** weighting between 5 and 10 mg were then obtained by the transport method already used for the preparations of $(Bu_4N)_2[Fe_4S_4(SPh)_4]$[6,7] and $(Et_4N)_2[Fe_4S_4(SCH_2Ph)_4]$.[8] In this method, a saturated solution of the compound **1** in acetonitrile is loaded in a tight tube under argon atmosphere in a temperature gradient. The temperature of the "hot" side of the tube is slowly decreased after an initial stay of some hours at a fixed maximum temperature.

We observed how important it was, in the case of this compound, to avoid heating the solution during the ligand exchange experiment. Besides, we observed that the maximum temperature during crystal growth must not exceed 50 °C. Otherwise, the solution turned dark gray, and crystals of compound **1** no longer grow. Instead, a black colloidal suspension appeared and single crystals of compound **3**, identified as a $(Et_4N)_2[Fe_2(SC_6H_4$-*o*-$O)_4]$ dimer, could eventually be formed.[15]

Crystals of compound **1** were afterward irradiated under argon atmosphere by γ-rays in a ^{60}Co source at room temperature, with doses varying between 0.2 and 0.5 MGy. The crystallographic structure of this compound has been published by Johnson et al.[13] It crystallizes in the monoclinic space group $P2_1/c$ ($\beta = 94.4°$) with $Z = 4$. The *bc* plane has been identified as one of easy cleavage. X-ray experiments based on the Laüe method were performed to determine the location of the *b* and *c* axes in the plane because they do not correspond to simple crystal edges. An orthogonal reference frame (*a**, *b*, *c*), with *a** defined as perpendicular to *b* and *c*, has then been devised from this morphology.

(2) EPR Methodology. The EPR spectra were obtained on a Bruker ER 200 D-SRC spectrometer, equipped with an Oxford Instruments ESR-9 continuous-flow helium cryostat. They were recorded in three perpendicular planes *a***b*, *bc*, and *ca**. Each paramagnetic center presents two inequivalent sites for a general orientation of the static magnetic field. When the magnetic field vector is either contained in the mirror glide plane *ca** or aligned along the *b* screw axis, these two sites become equivalent in the EPR spectra.

Experimental Results

Prior to γ-irradiation, it has been verified that the $[4Fe-4S]^{2+}$ single crystals used in this study were nearly free from paramagnetic impurities. After γ-irradiation, the EPR spectra reported for these single crystals showed the presence of numerous lines spread between $g = 1.80$ and $g = 2.15$, that is with relatively large (positional) anisotropies as a function of the orientation of the static field with respect to the crystal. These lines are associated with different paramagnetic species of spin angular momentum $S = {}^1/_2$. We have been able to follow the angular variations of 11 of these paramagnetic centers in three perpendicular planes *a***b*, *bc*, and *ca** previously defined. They are reported in Figure 2. These centers have been labeled from 1 to 9. Three of them, being very similar, received the labels 6, 6′, and 6″.

We have observed that the spin concentrations corresponding to these centers differ greatly. Moreover, the relative concentrations of the different centers can change substantially from one crystal to another. Their line widths are generally found to be roughly around 1 mT. For such a width, resolved hyperfine structures are therefore never observed. Consequently, following our previous studies,[7,10] we conclude that these paramagnetic species are not free radicals, which would have been created on the ligands or on the counterions, since they would rather exhibit much less anisotropic **g**-tensors and resolved proton hyperfine structure. In fact, the observed line widths are due to (nonresolved) proton hyperfine interactions with a spin population distribution which is mainly localized on the magnetic iron ions. This is clearly shown in the ENDOR study of one of these centers presented in Part 2. All the lines of these different centers vanish between 70 and 120 K, as very often observed for Fe−S centers. Most of these centers are relatively stable in the crystals at room temperature and remain visible by EPR during several months when stored at room temperature. However, centers 8 and 9 are less stable and they disappear in 1 month.

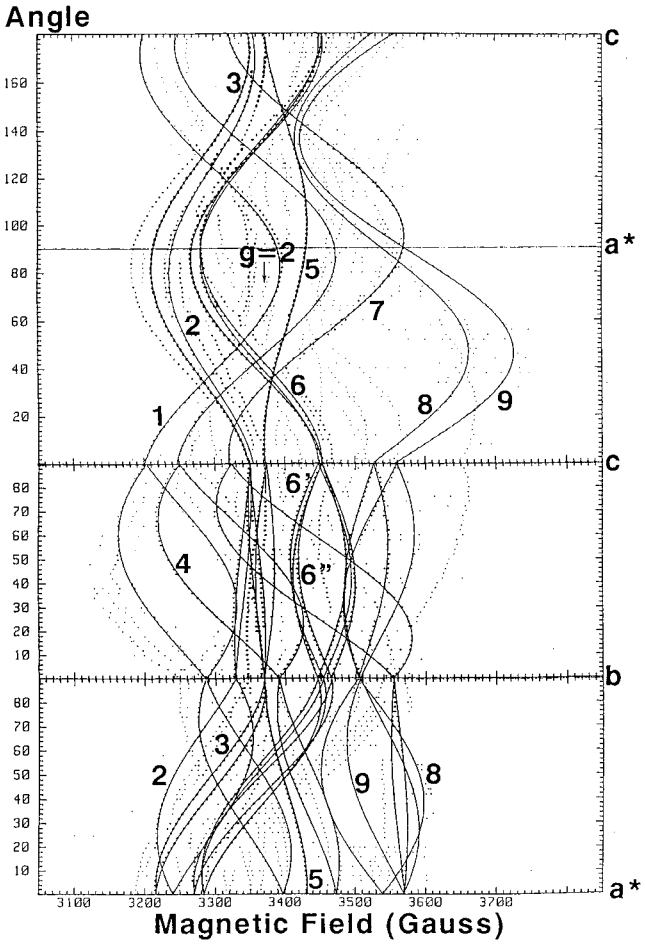

Figure 2. Angular dependences in the three orthogonal planes *a***b*, *bc*, and *ca** of the EPR lines corresponding to the different $[4Fe-4S]^{3+}$ and $[4Fe-4S]^{+}$ centers described in the text. The continuous curves represent computer fits.

From the experimental data presented in Figure 2, we calculated the **g**-tensors of these 11 centers. As is commonly done,[7,10] the experimental points were fitted by continuous curves corresponding to theoretical fits based on a Hamiltonian containing only the Zeeman interaction $\mathbf{H}\cdot\mathbf{g}\cdot\mathbf{S}$ with a spin angular momentum $S = {}^1/_2$:

$$[g_i(\theta)]^2 = U_i \cos^2\theta + V_i \sin^2\theta + 2W_i \sin\theta\cos\theta \quad (1)$$

where, for each plane *i*, the parameters U_i, V_i, and W_i are to be determined. The relative sign ambiguities of the off-diagonal terms of the **g**-tensors before diagonalization were resolved by

(14) Christou, G.; Garner, C. D. *J. Chem. Soc., Dalton Trans.* **1979**, 1093.
(15) Le Pape, L.; Excoffon, P.; Lamotte, B.; Laugier, J.; Rius, G. *New J. Chem.* **1997**, *21*, 231−235.

Table 1. Measured **g**-Tensors with Their Average Values, Eigenvalues, and Direction Cosines Relative to (*a**, *b*, *c*) Crystallographic Axes (as defined in ref 13)

no.	g_{av}	principal values	*a**	*b*	*c*
1	2.048	2.138	0.157	−0.508	−0.847
		2.028	−0.237	0.813	−0.532
		1.979	0.959	0.284	0.007
2	2.041	2.100	0.900	0.407	0.156
		2.014	−0.195	0.696	−0.691
		2.010	−0.390	0.591	0.706
3	2.038	2.101	0.990	0.056	0.127
		2.015	0.101	0.342	−0.934
		2.000	0.096	−0.938	−0.333
4	2.002	2.096	−0.023	−0.395	0.918
		1.974	0.371	−0.856	−0.359
		1.937	−0.928	−0.333	−0.166
5	1.989	2.010	0.095	−0.729	0.678
		1.994	−0.151	−0.684	−0.714
		1.965	0.984	−0.035	−0.175
6	1.989	2.058	0.986	0.162	−0.030
		1.976	0.137	−0.702	0.698
		1.933	−0.092	0.693	0.715
6′	1.988	2.057	0.992	0.127	0.022
		1.980	−0.068	0.663	−0.745
		1.929	−0.109	0.738	0.666
6″	1.988	2.065	0.996	0.063	0.062
		1.973	−0.006	−0.649	0.761
		1.926	0.088	−0.758	−0.646
7	1.939	2.045	0.085	0.291	0.953
		1.888	−0.985	−0.117	0.124
		1.884	−0.148	0.949	−0.277
8	1.914	1.980	0.715	0.317	−0.623
		1.936	0.042	0.870	0.491
		1.825	−0.697	0.378	−0.609
9	1.902	1.971	−0.688	−0.041	0.724
		1.932	−0.220	0.963	−0.154
		1.801	0.691	0.265	0.672

the determination of the **a**, **b**, and **c** directions using X-ray diffraction and, in addition, through the analysis of the angular variations of the EPR lines in a fourth plane intersecting the *a***bc* reference frame. The diagonalized **g**-tensors finally obtained are reported in Table 1. They are given for one site of the unit cell. By only changing all the signs of the direction cosines relative to the *b* axis, we can obtain the principal directions relative to the other magnetically inequivalent site. To compare, in what follows, the principal directions of these **g**-tensors to the most relevant atom−atom directions of the cubane, we have listed in Table 2 all angles between **Fe**−**Fe** directions and these principal directions ($\mathbf{V}_1$, $\mathbf{V}_2$, $\mathbf{V}_3$). These comparisons have been made in a systematic way for the two sets of solutions associated with the two inequivalent sites in the crystal. We have chosen here to present the results for the site corresponding to the most probable situation (those corresponding to the other situation are easily derivable from the crystallographic data and Table 1).

Discussion and Interpretation

Before analyzing the **g**-tensors of the different centers listed in Table 1, we wish to present in the following a theoretical model aiming at the general interpretation of both eigenvalues and principal directions of the **g**-tensors of the $[4Fe-4S]^{3+}$ and $[4Fe-4S]^{+}$ clusters. This model will be first discussed in the symmetric case and then, finally, when some asymmetry is introduced. Let us start by recalling some preliminary key features of these **g**-tensors.

(1) Theoretical Basis. In practice, two criteria of identification of the **g**-tensors are essential:

(i) the value of g_{av}, the average isotropic part of the **g**-tensor, allows us to distinguish between $[4Fe-4S]^{3+}$ and $[4Fe-4S]^{+}$ species. It is empirically established that $[4Fe-4S]^{3+}$ clusters have $g_{av} > g_e$ while $[4Fe-4S]^{+}$ ones have $g_{av} \leq g_e$, with $g_e \approx 2.0023$, the free electron *g*-factor (see for example ref 16 for a review of the **g**-tensors in the $[4Fe-4S]^{+}$ states).

(ii) the three eigenvalues ($g_1 \geq g_2 \geq g_3$) and their corresponding principal directions (among them, $\mathbf{V}_1$ being associated with the largest eigenvalue g_1) give some further information about the location of the two pairs of iron ions (six locations of the mixed-valence pair are possible, in principle, for a given structure). A good correlation between $\mathbf{V}_1$ and the common perpendicular of these two pairs has already been empirically established in the case of a nearly "symmetric" compound: $(Et_4N)_2[Fe_4S_4(SCH_2Ph)_4]$.[10]

We would like to understand the origin of such a correlation. As a general framework allowing us to adress this issue, let us see what are the main ingredients required for the calculation of **g**-tensors.

A first step consists of realizing that the **g**-tensor of a paramagnetic cluster of magnetically coupled transition metals can be expressed as a linear combination of "site" (or "monomer") $\mathbf{g}_i$-tensors of the individual uncoupled metal ions i ("i" stands formally for Fe^{2+}, $Fe^{2.5+}$, or Fe^{3+}):[17]

$$\mathbf{g} = \sum_{i=1}^{4} K_i \mathbf{g}_i \Rightarrow \Delta g_{av} = \sum_{i=1}^{4} K_i \Delta g_{i_{av}} \qquad (2)$$

In eq 2, $\Delta g_{av} = Tr(\Delta \mathbf{g})$ where $\Delta \mathbf{g} = \mathbf{g} - g_e \cdot \mathbf{Id}$ and K_i is the spin projection coefficient of the local spin $\vec{S}_i$ of the monomer *i* onto the total spin $\vec{S}$ of the cluster (with $\sum_i K_i = 1$):

$$K_i = \frac{\langle S_{iz} \rangle}{\langle S_z \rangle} \qquad (3)$$

The values of the $\{K_i\}$ depend themselves on the coupling scheme adopted for the ground state of the cluster. Previous analysis of $[4Fe-4S]^{3+}$ and $[4Fe-4S]^{+}$ centers showed that their most probable spin states are either $|^9/_2, 4, ^1/_2\rangle$ or $|^7/_2, 3, ^1/_2\rangle$. In these kets the first number is the spin of the two coupled iron atoms of the mixed-valence pair (each of the two ions will be referred to below as "mv"), the second one is the spin of the two coupled iron ions in the ferric ("3+") or ferrous ("2+") pair, and the last entry is the total spin of the cluster.[9,18−21] For the $|^9/_2, 4, ^1/_2\rangle$ state, $K_{mv} = +1.83$ for each of the two $Fe^{2.5+}$ sites of the (here delocalized) mixed-valence pair whereas K_{2+} $(=K_{3+}) = -1.33$ for each of the two ions (again supposed equivalent) of the ferrous or ferric pair. In the case of the $|^7/_2, 3, ^1/_2\rangle$ state, these coefficients are +1.50 and −1.00, respectively.

As a second step, and with eq 2 in mind, we now aim at deriving formal expressions for *site* tensors $\Delta\mathbf{g}(\mathbf{Fe}^{q+})$ ($q = 2$, 2.5, or 3), that is *local* quantities associated with *individual* iron sites. These local tensors are then combined to yield the total **g**-tensor of the system under study. As an illustration, starting for example from a low-spin broken symmetry state (made of four uncoupled high-spin monomers[22]), we will follow the procedure prescribed by Geurts et al.[23] (and applied for a [2Fe−

(16) Belinskii, M. *Chem. Phys.* **1993**, *172*, 189.
(17) Gibson, J. F.; Hall, D. O.; Thornley, J. H. M.; Whatley, F. R. *Proc. Natl. Acad. Sci. U.S.A.*. **1966**, *56*, 987.
(18) Middleton, P.; Dickson, D. P. E.; Johnson, C. E.; Rush, J. D. *Eur. J. Biochem.* **1978**, *88*, 135.
(19) Banci, L.; Bertini, I.; Briganti, F.; Luchinat, C.; Scozzafava, A.; Oliver, M. V. *Inorg. Chem.* **1991**, *30*, 4517.
(20) Bertini, I.; Campos, A. P.; Luchinat, C.; Teixeira, M. *J. Inorg. Biochem.* **1993**, *52*, 227.
(21) Mouesca, J.-M.; Noodleman, L.; Case, D. A.; Lamotte, B. *Inorg. Chem.* **1995**, *34*, 4347.
(22) Aizman, A.; Case, D. A. *J. Am. Chem. Soc.* **1982**, *104*, 3269.
(23) Geurts, P. J. M.; Bouten, P. C. P.; Avoird, A. v. d. *J. Chem. Phys.* **1980**, *73*, 1306.

Table 2. Comparison of the Eigenvalues of the "Asymmetric" Oxidized and Reduced Centers with Fe−Fe Based Directions

	oxidized center 1			oxidized center 2			oxidized center 3		
cryst directions	$\mathbf{V}_1$ (deg)	$\mathbf{V}_2$ (deg)	$\mathbf{V}_3$ (deg)	$\mathbf{V}_1$ (deg)	$\mathbf{V}_2$ (deg)	$\mathbf{V}_3$ (deg)	$\mathbf{V}_1$ (deg)	$\mathbf{V}_2$ (deg)	$\mathbf{V}_3$ (deg)
$Fe_1Fe_2-Fe_3Fe_4$	**03**	90	87	75	78	19	88	51	39
$Fe_1Fe_3-Fe_2Fe_4$	86	16	75	74	17	86	90	35	55
$Fe_1Fe_4-Fe_2Fe_3$	87	77	13	**20**	78	73	**03**	87	90
Fe_1Fe_2	88	**30**	60	63	33	73	45	57	62
Fe_1Fe_3	42	77	51	63	86	28	47	65	53
Fe_1Fe_4	48	44	79	70	55	**42**	90	81	**09**
Fe_2Fe_3	44	47	83	90	**36**	54	87	**08**	83
Fe_2Fe_4	48	81	44	33	74	62	43	66	56
Fe_3Fe_4	87	58	**32**	33	58	84	47	54	64

	reduced center 4			reduced center 5			reduced center 6		
cryst directions	$\mathbf{V}_1$ (deg)	$\mathbf{V}_2$ (deg)	$\mathbf{V}_3$ (deg)	$\mathbf{V}_1$ (deg)	$\mathbf{V}_2$ (deg)	$\mathbf{V}_3$ (deg)	$\mathbf{V}_1$ (deg)	$\mathbf{V}_2$ (deg)	$\mathbf{V}_3$ (deg)
$Fe_1Fe_2-Fe_3Fe_4$	55	38	77	79	19	75	88	78	12
$Fe_1Fe_3-Fe_2Fe_4$	**32**	61	78	**11**	81	84	79	14	81
$Fe_1Fe_4-Fe_2Fe_3$	88	74	16	84	75	16	**08**	82	89
Fe_1Fe_2	52	54	59	38	89	52	55	36	81
Fe_1Fe_3	71	**37**	60	89	60	**30**	44	89	46
Fe_1Fe_4	78	20	74	53	38	81	86	55	**35**
Fe_2Fe_3	11	79	88	36	58	77	82	**35**	57
Fe_2Fe_4	65	68	**34**	79	**31**	61	48	76	45
Fe_3Fe_4	56	79	36	52	71	44	37	55	81

	reduced center 7			reduced center 8			reduced center 9		
cryst directions	$\mathbf{V}_1$ (deg)	$\mathbf{V}_2$ (deg)	$\mathbf{V}_3$ (deg)	$\mathbf{V}_1$ (deg)	$\mathbf{V}_2$ (deg)	$\mathbf{V}_3$ (deg)	$\mathbf{V}_1$ (deg)	$\mathbf{V}_2$ (deg)	$\mathbf{V}_3$ (deg)
$Fe_1Fe_2-Fe_3Fe_4$	**18**	82	74	64	30	76	49	67	50
$Fe_1Fe_3-Fe_2Fe_4$	73	78	21	50	64	51	62	29	82
$Fe_1Fe_4-Fe_2Fe_3$	79	12	84	47	82	44	51	81	40
Fe_1Fe_2	72	56	**39**	88	75	15	82	39	52
Fe_1Fe_3	58	39	70	42	57	68	28	63	85
Fe_1Fe_4	63	90	27	82	20	71	81	21	71
Fe_2Fe_3	31	78	62	44	73	51	40	70	57
Fe_2Fe_4	37	54	83	80	44	48	88	80	10
Fe_3Fe_4	87	**37**	53	26	64	87	43	59	64

$2S]^+$ cluster[24]) by restricting the molecular orbitals involved to their *individual* iron parts (including the MO coefficients) to estimate the *site* $\Delta\mathbf{g}(\mathbf{Fe}^{q+})$'s.

Let us therefore consider the general expression of the g_{mn} element of a site $\mathbf{g}_i$-tensor, with $\{m,n\} \in \{x,y,z\}$ (the reference frame will be defined more precisely below). It implies the promotion of electron(s) in occupied molecular spin−orbital(s) $|o\rangle$ (of energy ϵ_o) into corresponding empty spin−orbital(s) $|p\rangle$ (of same spin and of energy ϵ_p) lying above ($\epsilon_p > \epsilon_o$), as written in eq 4. The spin−orbit coefficient λ is taken here as

$$g_{mn} = g_e + 2\lambda\left(\sum_{\alpha} - \sum_{\beta}\right)\left(\sum_{o}\sum_{\substack{p \\ (\epsilon_p>\epsilon_o)}} \frac{\langle o|L_m|p\rangle\langle p|L_n|o\rangle}{\epsilon_p - \epsilon_o}\right) \quad (4)$$

positive, and the contributions of α and β spins have opposite signs. The literature[25−27] of the spectroscopy of *individual* Fe^{2+} and Fe^{3+} ions shows that $\Delta g(Fe^{2+})_{av}$ is positive (around 0.10) while $\Delta g(Fe^{3+})_{av}$ turns out to be most often positive, but much smaller (around 0.01−0.04). We do not have a direct way of measuring these quantities in *coupled* systems. But the shift Δg_{av} of the trace of the total **g**-tensor from the free electron value can still be traced back in principle to the corresponding shifts at the level of the most "reduced" site (in the sense of containing the most ferrous contribution, i.e., $Fe^{2.5+}-Fe^{2.5+}$ in $[4Fe-4S]^{3+}$ but $Fe^{2+}-Fe^{2+}$ in $[4Fe-4S]^{+}$). On account of that fact, and because of the opposite signs of the spin projection coefficients ($K_{mv} > 0$ whereas K_{2+}, $K_{3+} < 0$), we can rationalize, from eq 2, the deduction of point i above.

(2) Theoretical Model for the g-Tensors of the $[4Fe-4S]^{3+}$ and $[4Fe-4S]^{+}$ States. We will consider first a *symmetric* cluster, i.e., a cluster for which the iron atoms in both the mixed-valence pair, aligned here along **x**, and the ferric—or ferrous—pair, along **y**, are equivalent; this corresponds to a C_{2v} symmetry of the electronic structure and the same, or even higher (i.e., D_{2d}), symmetry for the nuclear frame (with **z**, the main C_2 axis, being perpendicular to both mixed-valence and ferric/ferrous pairs).

(a) Electronic Energy Diagrams of the $[4Fe-4S]^{3+}$ and $[4Fe-4S]^{+}$ States. Made after similar previously published diagrams,[22,28−30] the *schematic* spin−orbital energy diagram based on density functional calculations is shown in Figure 3 for $[4Fe-4S]^{3+}$ and in Figure 4 for $[4Fe-4S]^{+}$. Three distinct set of orbitals are clearly distinguishable in Figure 3. From top to bottom, the first set comprises mostly empty orbitals, *mainly* of iron character (only the lowest level is occupied in the case of a mixed-valence pair, the two lowest for a ferrous pair; see Figure 4). They form 10 (metal−metal) bonding/antibonding d orbitals. The second set lies below the HOMO (i.e., is filled) and is mostly of ligand (S,S*) character (with some *minor* iron content). Finally, the mixing and splitting invoked within the first metal set applies as well within the majority spin iron levels forming the third set. The level pattern in which the S,S*(3p) ligand orbitals (here of both spin) are "sandwiched" between Fe(3d) majority spin (lower) and Fe-(3d) minority spin (higher) orbitals is called the "inverted level scheme" (in the "normal" level scheme, the occupied ligand levels are below the metal one). This has been systematically found computationaly for $[Fe(SR)_4]^{1-,2-}$, $[Fe_2S_2(SR)_4]^{2-,3-}$, and $[Fe_4S_4(SR)_4]^{1-,2-,3-}$ iron−sulfur complexes.[22,24,28,31−33] This scheme has also been demonstrated experimentally for ferric ions in $[FeCl_4]^{-}$ [34] and $[FeS_4]^{5-}$ [34,35] systems as well as for a

(24) Noodleman, L.; Baerends, E. J. *J. Am. Chem. Soc.* **1984**, *106*, 2316.

(25) Schultz, C.; Debrunner, P. G. *J. Phys. Colloq.* **1976**, *37*, 153.

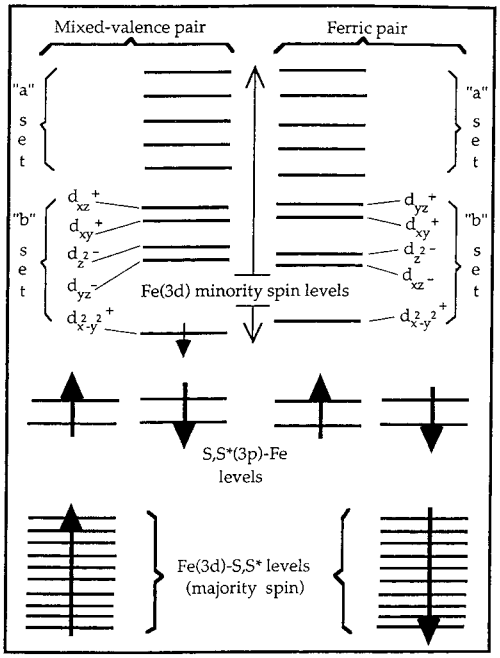

Figure 3. Full schematic spin−orbital energy diagram for $[Fe_4S_4(SR)_4]^{1-}$ anions.

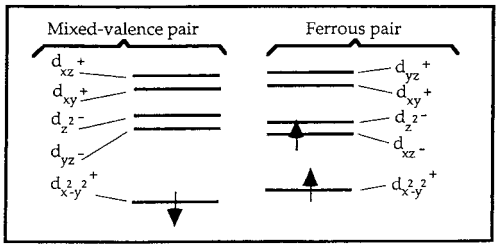

Figure 4. Partial schematic spin−orbital energy diagram for $[Fe_4S_4(SR)_4]^{3-}$ anions representing only the five lowest ("bonding") molecular orbitals for each pair (OC2 configuration).

tetrathiolate model $[Fe(SR)_4]^-$.[36] An analogous work[37] has been performed for the corresponding reduced model compound $[Fe(SR)_4]^{2-}$, although revealing in that case more mixing between iron and sulfur levels than in the ferric case.

(b) Qualitative Foundations of the Energy Diagrams: from Monomers to the Tetramer, via Dimers. We depict in Figure 5 the setting up, at the level of a pair (here "12" for example), of this schematic energy level diagram. The parts pertaining to the individual iron sites 1 and 2 (referred to by I, II, and III) correspond to spin-unrestricted bonding schemes[36] of high-spin iron complexes.[34,35,37] In I are represented the 10

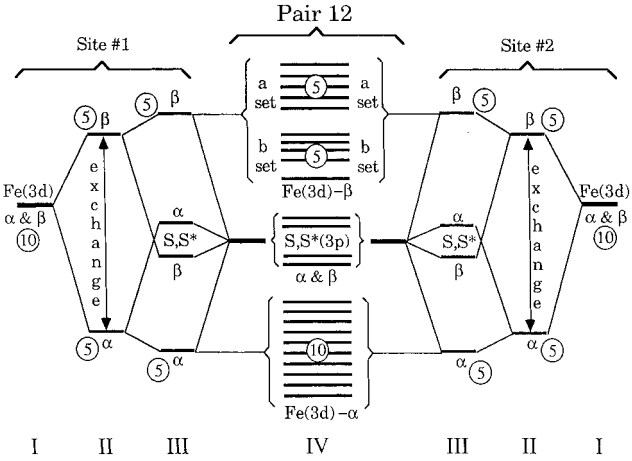

Figure 5. Setting up of the "inverted"level scheme (IV: cf. Figure 3) as a result from exchange polarization between α and β spin levels (from I to II) and subsequent mixing of the metal and ligand orbitals (from II to III). The whole I−III part of the diagram, covering individual sites, has been demonstrated experimentally by Solomon et al.[34−37]

(five α and five β) degenerate atomic d orbitals of the free iron ion. On going from I to II, spin polarization is "turned on", splitting occupied α-spin−orbitals below the empty (in Fe^{3+}) β-spin−orbitals (by around 4−5 eV for Fe^{3+}[33]). This exchange energy being much larger than the ligand field stabilization energy (10 Dq ∼ 0.5 eV),[36,37] the iron ions are high-spin.

In step III of Figure 5 is depicted the result of the mixing of metal and ligand levels, yielding, in order of increasing energy, majority (mainly iron) spin-α levels (which could be qualified as well as metal−ligand weakly/strongly antibonding[33]), ligand levels and minority (mainly iron) spin-β levels. We find at this stage the building up of the inverted level scheme referred to above. We would find here an additional splitting of the metal levels due to ligand field effects (not represented in Figure 5). What will be the relative energetic order within the minority spin set ("b" and "a" of Figure 3) can be appreciated by appealing to the angular overlap method (AOM: see a description of this approximation for example in Burdett[38]). This method allows us namely to deal with the influence of the sulfur environment (ligand field effects) on the relative energies of the atomic d orbitals in a semiquantitative fashion.

(i) The Monomers. In Figure 6a is represented one iron ion surrounded by four equivalent ligands in tetrahedral coordination. In [4Fe−4S] clusters, three out of the four ligands are formal S^{2-} inorganic sulfur ions, of close shell configuration $[3s^23p^6]$. We will consider therefore a first system made of one Fe^{3+} and four S^{2-}. In the *local* reference system $\{\mathbf{x}',\mathbf{y}',\mathbf{z}'\}$ suitable for the description of ligand field effects within a tetrahedron (i.e., with the axes perpendicular to the faces of the cube), the five atomic d orbitals are split into the **e** set ($d_{x'^2-y'^2}$,$d_{z'^2}$) of energy ($^8/_3e_\pi$) and the $\mathbf{t}_2$ set ($d_{x'y'}$, $d_{x'z'}$, and $d_{y'z'}$) of energy ($^4/_3e_\sigma + {}^8/_9e_\pi$).[38] Here e_σ and e_π are σ (along the metal−ligand bond) and π (perpendicular to that bond) interaction energies ($e_\sigma \sim 0.5$ eV and $e_\sigma \sim 5e_\pi$).[38] In this picture, the ligand field orbital splitting is calculated as being 10 Dq ≡ $(4/3)e_\sigma - (16/9)e_\pi$ (∼0.5 eV).

In Figure 6b is represented an iron dimer made of two of the preceding monomers. Such a dimer is actually found (although distorded) in [4Fe−4S] cubanes. For the sake of simplicity, we suppose at first that the ligand environment of the two iron ions is still of tetrahedral symmetry. We go then from the *local* (Figure 6a) to the *global* (Figure 6b) system of axes {**x**,**y**,**z**} (same as defined above for tetramers) by a clockwise rotation

(26) Moura, I.; Huynh, B. H.; Hausinger, R. P.; LeGall, J.; Xavier, A. V.; Münck, E. *J. Biol. Chem.* **1980**, *255*, 2493.
(27) Papaefthymiou, V.; Girerd, J.-J.; Moura, I.; Moura, J. J. G.; Münck, E. *J. Am. Chem. Soc.* **1987**, *109*, 4703.
(28) Noodleman, L.; Norman, J. G.; Osborne, J. H.; Aizman, A.; Case, D. A. *J. Am. Chem. Soc.* **1985**, *107*, 3418.
(29) Noodleman, L.; Case, D. A.; Baerends, E. J. In *Density Functional Methods in Chemistry*; Labanowski, J. K., Andzelm, J. W., Eds.; Springer-Verlag: New-York, 1991; pp 109−123.
(30) Noodleman, L. *Inorg. Chem.* **1991**, *30*, 246.
(31) Norman, J. G.; Jackels, S. C. *J. Am. Chem. Soc.* **1975**, *97*, 3833.
(32) Norman, J. G.; Ryan, P. B.; Noodleman, L. *J. Am. Chem. Soc.* **1980**, *102*, 4279.
(33) Noodleman, L.; Peng, C. Y.; Case, D. A.; Mouesca, J.-M. *Coord. Chem. Rev.* **1995**, *144*, 199.
(34) Butcher, K. D.; Didziulis, S. V.; Briat, B.; Solomon, E. I. *J. Am. Chem. Soc.* **1990**, *112*, 2231.
(35) Butcher, K. D.; Gebhard, M. S.; Solomon, E. I. *Inorg. Chem.* **1990**, *29*, 2067.
(36) Gebhard, M. S.; Deaton, J. C.; Koch, S. A.; Millar, M.; Solomon, E. I. *J. Am. Chem. Soc.* **1990**, *112*, 2217.
(37) Gebhard, M. S.; Koch, S. A.; Millar, M.; Devlin, F. J.; Stephens, P. J.; Solomon, E. I. *J. Am. Chem. Soc.* **1991**, *113*, 1640.
(38) Burdett, J. K. *Molecular Shapes. Theoretical Models of Inorganic Stereochemistry*; Wiley: New York, 1980.

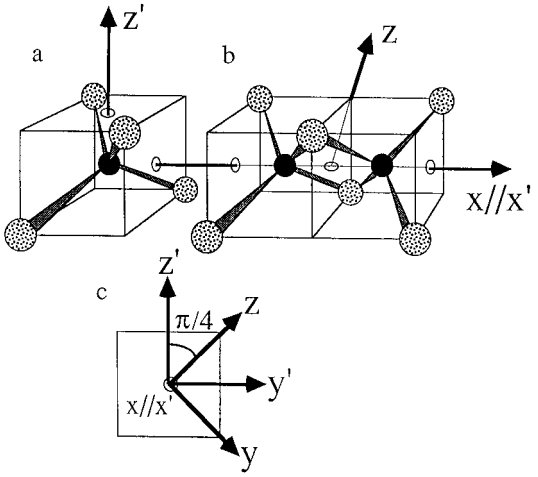

Figure 6. (a) Definition of the "local" axis system {**x**′,**y**′,**z**′} for an iron ion tetrahedrically ligated to four equivalent ligands (i.e., sulfur atoms). These axes are perpendicular to the cube faces, **x**′ pointing to the right (**y**′ is not drawn, but points to the back). (b) Definition of the "global" axis system {**x**,**y**,**z**} having **x** = **x**′ in common with the previous reference frame. The system devised for the dimer here is the same as that used for tetramers (see main text). (c) Second frame (unprimed axis labels) deduced from the first one (primed axis labels) by a clockwise rotation of $\pi/4$ aroud **x** = **x**′.

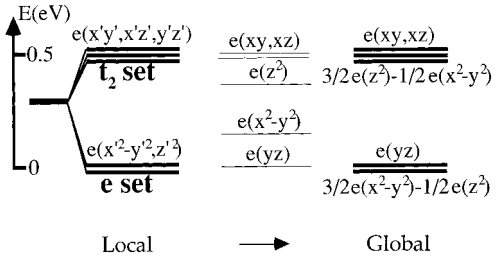

Figure 7. Changes, in the labeling, of the atomic d orbitals when passing from "local" to "global" coordinates.

of $\pi/4$ around **x** = **x**′ (see Figure 6c). The **x** axis thus remains along the Fe−Fe direction while the **z** axis is made perpendicular to the central Fe_2S_2 face. We can now express the atomic d orbitals from global into local coordinates and calculate their energies according to the AOM:[38,39]

$$\begin{cases} d_{x^2-y^2} = +\frac{3}{4}d_{x'^2-y'^2} - \frac{\sqrt{3}}{4}d_{z'^2} + \frac{1}{2}d_{y'z'} \\ d_{z^2} = -\frac{\sqrt{3}}{4}d_{x'^2-y'^2} + \frac{1}{4}d_{z'^2} + \frac{\sqrt{3}}{2}d_{y'z'} \\ d_{xy} = +\frac{\sqrt{2}}{2}d_{x'y'} - \frac{\sqrt{2}}{2}d_{x'z'} \\ d_{xz} = +\frac{\sqrt{2}}{2}d_{x'y'} + \frac{\sqrt{2}}{2}d_{x'z'} \\ d_{yz} = -\frac{1}{2}d_{x'^2-y'^2} - \frac{\sqrt{3}}{2}d_{z'^2} \end{cases} \Rightarrow \begin{cases} e(d_{x^2-y^2}) = \frac{1}{3}e_\sigma + \frac{20}{9}e_\pi \\ e(d_{z^2}) = e_\sigma + \frac{4}{3}e_\pi \\ e(d_{xy}) = \frac{4}{3}e_\sigma + \frac{8}{9}e_\pi \\ e(d_{xz}) = \frac{4}{3}e_\sigma + \frac{8}{9}e_\pi \\ e(d_{yz}) = \frac{8}{3}e_\pi \end{cases} \quad (5)$$

As it turns out for such a tetrahedral environment, if $d = \sum_i c_i d_i'$ (cf. eq 5), then $e(d) = \sum_i c_i^2\, e(d_i')$, with $e(d_i')$ depending on e_σ and e_π as explicited above.

In Figure 7 is represented the change in atomic energies and characters on going from local to global reference systems. The energies of the d′ orbitals of the **e** and $\mathbf{t}_2$ sets are thus redistributed among the "new" unprimed d orbitals. The relative energetic ordering of the d orbital levels does not depend on the choice of axes: mixing must occur between the $d_{x^2-y^2}$ and d_{z^2} orbitals to ensure this constraint. One thus finds $e(d_{xy},d_{xz}) = {}^3/_2 e(d_{z^2}) - {}^1/_2 e(d_{x^2-y^2})$ and $e(d_{yz}) = {}^3/_2 e(d_{x^2-y^2}) - {}^1/_2 e(d_{z^2})$. We notice that (i) $d_{x'y'}$ and $d_{x'z'}$ go into d_{xy} and d_{xz} without change of energy (cf. eq 5), (ii) the former **e** set is now split, with the new $d_{x^2-y^2}$ (mixed with d_{z^2}) lying below, and (iii) d_{yz} is now in the lower set of the five "new" atomic orbitals. We expect of course that the presently derived relative ordering of the d orbitals be somewhat perturbed by different factors, among which are (i) lowering of the global (and/or local, i.e., at the iron sites) symmetry of the cluster and (ii) the chemical difference between cysteinyl and inorganic sulfur atoms breaking the local T_d symmetry. By replacing only one inorganic sulfur S^{2-} by one thiolate sulfur RS^-, we expect little change in Figure 7, apart from splitting of the two **e** and $\mathbf{t}_2$ sets, in (iii) the role played by the orientation of the 3p valence orbital of the ligand sulfur due to rotation of the Fe−S−R group around Fe−S,[36,37] which is important in the case of one iron surrounded by *four* cysteinyl ligands.

(ii) Orbital Overlaps inside the Dimer. By building up the dimer from the adjunction of two monomers, a new feature has to be considered, i.e., the direct (through-space) interaction of the metal d orbitals. These are now discussed in the case of a bare (without sulfur ligands) Fe−Fe dimer (step IV of Figure 5). Before relying again on AOM[38] to estimate overlaps between pairs of atomic d orbitals, let us describe the symmetry constraints relevant to their mixing and splitting. Let us start our analysis by considering five (minority spin β) d orbitals ($d^1_{x^2-y^2}$, $d^1_{z^2}$, d^1_{xy}, d^1_{xz}, and d^1_{yz}) located on site 1, expressed in the *global* reference system {**x**,**y**,**z**} corresponding to the C_{2v} symmetry. Again, the **z** axis is the main C_2 axis whereas, most importantly for what follows, the **x** axis is directed along the mixed-valence pair. We build then (cf. going from III to IV in Figure 5) five (metal−metal) *bonding* and five *antibonding* linear combinations of those atomic spin−orbitals (for example $d_{x^2-y^2}{}^+ = 2^{-1/2}\{d^1_{x^2-y^2} + d^2_{x^2-y^2}\}$). These 10 orbitals are distributed among the four C_{2v} symmetries in the following manner: $\mathbf{d}_{x^2-y^2}{}^+$, $d_{z^2}{}^+$, and $d_{xz}{}^-$ in A_1, $\mathbf{d}_{yz}{}^-$ and $\mathbf{d}_{xy}{}^+$ in A_2, $\mathbf{d}_{z^2}{}^-$, $\mathbf{d}_{xz}{}^+$, and $d_{x^2-y^2}{}^-$ in B_1, and $d_{xy}{}^-$ and $d_{yz}{}^+$ in B_2. In boldface are distinguished the five lowest of those molecular spin−orbitals (cf. Figure 3), already qualified as "bonding" (caution here: the minus signs do appear among the "bonding" MO's $d_{yz}{}^-$ and $d_{z^2}{}^-$ because of the use of the common *global* reference system). The +/− signs used here in $d^{+/-}$ are the symmetric/antisymmetric phases of the pairwise delocalized MO's. Upon going from one pair (i.e., mixed-valence) to the other one (ferric/ferrous) in the cubane, remember that $x \leftrightarrow y$ and $B_1 \leftrightarrow B_2$, that is $d_{x^2-y^2}{}^+$, $d_{z^2}{}^+$, and $d_{yz}{}^-$ are found in A_1, $d_{xz}{}^-$ and $d_{xy}{}^+$ in A_2, $d_{xy}{}^-$ and $d_{xz}{}^+$ in B_1 and $d_{z^2}{}^-$, $d_{yz}{}^+$, and $d_{x^2-y^2}{}^-$ in B_2 on the side of the ferric/ferrous pair; see again Figure 3.

Applying AO methods for the semiquantitative treatment of the d−d splitting, we find that[38]

$$\begin{cases} E(d_{x^2-y^2}) = \frac{3}{4}E_\sigma + \frac{1}{4}E_\delta \\ E(d_{z^2}) = \frac{1}{4}E_\sigma + \frac{3}{4}E_\delta \\ E(d_{xy}) = E_\pi \\ E(d_{xz}) = E_\pi \\ E(d_{yz}) = E_\delta \end{cases} \quad (6)$$

where the E(d)'s are the d−d splitting energies, expressed in terms of $E_{\sigma,\pi,\delta}$, splitting energies of σ, π, and δ type. To get relative estimates of these quantities, we performed a very simple density funtional calculation, converging the electronic structure of a bare (without ligand) "high-spin" ($S = {}^9/_2$) Fe_2 dimer (d(Fe−Fe) = 2.75 Å) in the global coordinate system (with Fe−Fe along **x**). The Amsterdam density functional code[40−42] has been utilized, with LDA of Vosko, Wilk, and Nusair[43] and nonlocal corrections to the exchange (Becke[44]) and

(39) Gerloch, M.; Slade, R. C. *Ligand-Field Parameters*; University Press: Cambridge, U.K., 1973.

(40) Baerends, E. J.; Ellis, D. E.; Ros, P. *Chem. Phys.* **1973**, *2*, 41.
(41) Baerends, E. J.; Ros, P. *Chem. Phys.* **1973**, *2*, 52.
(42) Baerends, E. J.; Ellis, D. E.; Ros, P. *J. Comput. Phys.* **1992**, *99*, 84.

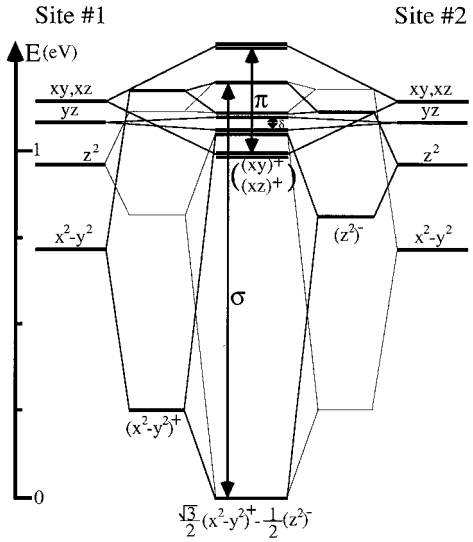

Figure 8. Energy level diagram obtained for a bare Fe_2 dimer (DF calculation) showing the mixing (according to C_{2v} symmetry) and splitting of the d atomic orbitals. The Fe−Fe direction is defined as **x**. Are also represented by vertical arrows the amount of σ (mixture of x^2-y^2 and z^2 orbitals maximizing the overlap along **x**), π (*xy* and *xz* orbitals), and δ (*yz* orbitals perpendicular to **x**) bonding−antibonding interaction energies ($E_{\sigma,\pi,\delta}$ in the main text). By reconstruction of the sites 1 and 2 atomic orbitals, the five d energies do not coalesce because of the use of the angular overlap method (see main text) to analyze the DFT-derived d−d splittings, both theories resting on different approximations.

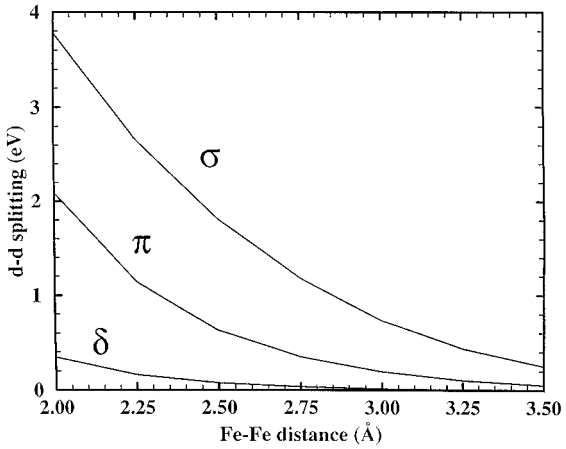

Figure 9. σ, π, and δ bonding−antibonding interaction energies as a function of the Fe−Fe distance. Over the whole calculated range 2.00−3.50 Å, $3 < E_\sigma/E_\pi < 4$ and $8 < E_\pi/E_\delta < 12$.

the correlation (Perdew[45]). The orbital energy diagram obtained is represented in Figure 8. The d−d splittings calculated for the d_{xy}, d_{xz}, and d_{yz} orbitals yield straightforwardly $E_\pi \sim 2800$ cm^{-1} (0.35 eV) and $E_\delta \sim 300$ cm^{-1} (0.04 eV). For the two last orbitals ($d_{x^2-y^2}$ and d_{z^2}), mixing occurs, resulting in maximal bonding energy. In effect, the interaction energy of the mixed orbital $d_{x^2-y^2}^* = \cos\theta\, d_{x^2-y^2} + \sin\theta\, d_{z^2}$ is calculated to be $E(d_{x^2-y^2}^*) = \cos^2(\theta + \pi/6)E_\sigma + \sin^2(\theta + \pi/6)E_\delta$. This is maximal for $\theta = -\pi/6$, where $E_{max}(d_{x^2-y^2}^*) = E_\sigma \sim 9600$ cm^{-1} ($\sim$1.2 eV). Another way to look at it is the following: with **z″** along the Fe−Fe direction, the mixed orbital $d_{x^2-y^2}^*$ transforms into $\cos(\theta + \pi/6)d_{z''^2} + \sin(\theta + \pi/6)d_{x''^2-y''^2}$, that is into a "pure" $d_{z''^2}$ orbital for $\theta = -\pi/6$. This is indeed the mixing angle appearing at the bottom of Figure 8, i.e., $\cos(-\pi/6) = 3^{1/2}/2$, $\sin(-\pi/6) = -1/2$. Then, for the same optimal value of θ, $E(d_{z^2}^*) = \sin^2(\theta + \pi/6)E_\sigma + \cos^2(\theta + \pi/6)E_\delta$ (with $d_{z^2}^* = -\sin\theta\, d_{x^2-y^2} + \cos\theta\, d_{z^2}$) reaches its *minimal* value, that is E_δ.

It is interesting to notice that θ depends, in iron−sulfur clusters, on the S-cysteine bond orientation about the Fe−S axis; thus, θ can depart slightly from $-\pi/6$, thus adding into the $d_{z''^2}$ orbital a small amount of $d_{x''^2-y''^2}$ character.[24,28,46] Moreover, this addition will also rapidly increase the value of $E(d_{z^2}^*)$ because of the large value of E_σ. Finally, in Figure 9, we plot the variations of $E_{\sigma,\pi,\delta}$ as a function of the Fe−Fe distance to verify that, say over the range 2.5−3.0 Å (relevant for most iron−sulfur systems), $3 < E_\sigma/E_\pi < 4$ and $8 < E_\pi/E_\delta < 12$. This Figure 9 is analogous to Figure 4 of ref 47 where σ, π, and δ orbital overlaps are sketched. We verified that almost the same diagram is obtained for ferric and ferrous pairs (not shown).

As stated at the introduction of this section, the main features of the relative ordering of the molecular orbitals in Figure 3 can be thus derived by putting together the semiquantitative results deduced from Figure 7 and Figure 8. Due to dominant σ interaction of $d_{x^2-y^2}$ (and small δ interaction of d_{yz}), the combination $d_{x^2-y^2}^+$ becomes the HOMO in the mixed-valence pair (or, equivalently, LUMO in the ferric pair). The (d_{xy},d_{xz}) orbitals are expected to remain close energetically, as found computationally. From the discussion of the previous paragraph, we expect some σ contribution to the $d_{z^2}-d_{z^2}$ bonding scheme, thus bringing the combination $d_{z^2}^-$ close to d_{yz}^-.

Finally, some interchange of iron molecular orbitals can also occur at the border between the "b" and "a" sets (see Figure 3) without affecting the results of our discussion on the **g**-tensor (see an illustration of that interchange in Figure 3 and/or Figure 4 of ref 29, where the upper right quarter of Figure 3 is there detailed for $[4Fe-4S]^{2+}$: the $15b_1$ xz^+ orbital lies relatively low within the "b" set due to the very small E_δ in Fe_2, or, equivalently, to small $10B_\delta$ in Fe_4S_4).

Going back now to Figure 3, we have argued for the fact that, among the 10 spin−orbitals of the Fe(3d) minority spin levels, delocalized over this iron pair, the lowest one is expected to be $|o\rangle = |d_{x^2-y^2}^+\rangle$ (of energy ϵ_o). In the mixed-valence pair, $|o\rangle$ is actually occupied by the "sixth" d electron of the former (that is "before" delocalization) ferrous ion, thus resulting in two formal $Fe^{2.5+}$ ions. This feature turns out to be the *key* point for the understanding of the $\Delta\mathbf{g}$ tensors in $[4Fe-4S]^{3+}$ clusters. This delocalized electron (*minority* spin $s = 1/2$) is antiparallel to the spin 5 of the *majority* spin of its iron pair (hence of resulting spin $S_{mv} = 5 - 1/2 = 9/2$). The energetic gap between this occupied orbital and the empty ones of the "b" set, grouped within about 0.6−0.7 eV, is about 1 eV.[22,28−30]

To conclude, a schematic diagram equivalent to that of Figure 5 can be set up for the other pair of iron atoms "34" simply by permuting α and β spin levels. Minority spin levels of both pairs are of opposite spin (reflecting the fact that, in the tetramer, the two pairs are *antiferromagnetically* coupled). Moreover, within a given spin set (α or β), negligible mixing is expected between majority spin levels of one pair and minority spin levels of the other pair because of the large energetic gap between the two sets of levels (cf. inverted level scheme). The diagram in the figure can be therefore used directly to describe qualitatively the iron pair in a tetramer. For the other pair (ferric in Figure 3, ferrous in Figure 4), one obtains an equivalent description and distribution but, again, by permuting "*x*" and "*y*" subscripts as well as B_1 and B_2 symmetry representations. In the case of the *ferrous* pair, we notice at the outset that more care has to be taken for the calculation of the matrix element involving the two quasi-degenerate orbitals d_{xz} and d_{z^2} (we will

(43) Vosko, S. H.; Wilk, L.; Nusair, M. *Can. J. Phys.* **1980**, *58*, 1200.
(44) Becke, A. D. *Phys. Rev.* **1988**, *A38*, 3098.
(45) Perdew, J. P. *Phys. Rev.* **1986**, *B33*, 8822.
(46) Bertrand, P.; Gayda, J.-P. *Biochim. Biophys. Acta* **1979**, *579*, 107.
(47) Trogler, W. C. *J. Chem. Educ.* **1980**, *57*, 424.

come back to this point later on). Let us now derive the $\Delta g(Fe^{q+})$'s and thus the $\Delta\mathbf{g}$ tensors for the two redox states.

(3) g-Tensor Model for the [4Fe−4S]$^{3+}$ State. (a) Symmetric Case. As far as an explicit derivation of the expression of the **g**-tensor is concerned, and starting with the mixed-valence pair, let us consider at once the two sets of (metal−metal) bonding ("b") and antibonding ("a") orbitals (here at first made of "pure" iron d orbitals; the effect of introducing sulfur orbitals will be considered later). The calculation of the mixed-valence pair contribution to the **g**-tensor implies the promotion of the electron in $d_{x^2-y^2}{}^{+}$ into the four symmetric (+) empty orbitals p (of energy $\epsilon_p{}^{mv}$) lying above, namely, $d_{yz}{}^{+}$, $d_{z^2}{}^{+}$, $d_{xy}{}^{+}$, and $d_{xz}{}^{+}$. Taking into account the phases introduces implicitly a selection rule for the d−d transitions relevant to the calculation of $\Delta\mathbf{g}(\mathbf{Fe^{2.5+}})$, i.e., here transitions within the set of symmetric orbitals (let us recall again that we are calculating *site* tensors, i.e., that we extract from these symmetric orbitals the part pertaining to an *individual* ion). We notice also that, for the construction of our *qualitative* model, the knowledge of the exact energies of the orbitals is not that relevant, but only the fact that the electron to be promoted occupies an orbital of $d_{x^2-y^2}$ character and that the four other empty orbitals are somewhat "grouped" above this occupied one (cf. point ii below).

Using the modes of operation of $\mathbf{L_x}$, $\mathbf{L_y}$, and $\mathbf{L_z}$ on the real forms of the d-functions, one can then calculate at once the contribution to $\Delta\mathbf{g}(\mathbf{Fe^{2.5+}})$ expressed in the (**x**,**y**,**z**) basis. One can now write $\Delta\epsilon_{xy} = \epsilon_{xy}{}^{mv} - \epsilon_{x^2-y^2}{}^{mv}$ ($\Delta\epsilon_{xz} = \epsilon_{xz}{}^{mv} - \epsilon_{x^2-y^2}{}^{mv}$, and $\Delta\epsilon_{yz} = \epsilon_{yz}{}^{mv} - \epsilon_{x^2-y^2}{}^{mv}$):

$$\Delta g(Fe^{2.5+}) = K_{mv} \times \left(\frac{2\lambda}{4}\right) \times \begin{pmatrix} \frac{1}{\Delta\epsilon_{yz}} & 0 & 0 \\ 0 & \frac{1}{\Delta\epsilon_{xz}} & 0 \\ 0 & 0 & \frac{4}{\Delta\epsilon_{xy}} \end{pmatrix} \quad (7)$$

We notice in eq 7 that the orbital of d_{z^2} character does *not* contribute in this calculation, all of the corresponding matrix elements of $\mathbf{L}_m$ $\{m = x, y, z\}$ with $d_{x^2-y^2}$ being zero. Moreover, still ignoring metal−ligand mixing (i.e., dealing for the moment with "pure" d iron orbitals), the filled majority spin α orbitals have no counterpart empty orbitals to which their electrons could be promoted: only minority spin−orbitals intervene in the calculation of local tensors. As a striking illustration of this neglect, $\Delta g(Fe^{3+})$ would be equal to 0.0 since there is no minority spin α electron to be promoted at all at the level of the ferric site.

The mixing (within the restrictions imposed by the symmetry of the electronic structure), depicted in step III of Figure 5, between the iron d orbitals and the ligand orbitals (mainly the sulfur atoms S, S*) manifests itself in two closely related ways. It results first in *covalency* effects. For the highest occupied molecular orbital $|o\rangle$, for example, the weight of the iron orbital-(s) $d_{x^2-y^2}$ translates into a covalency factor of about $D_{x^2-y^2} \sim 80\%$. Let us recall here that, neglecting overlap, this covalency factor is the square of the coefficient of the "atomic" orbital $d_{x^2-y^2}$ contained in the molecular orbital $|o\rangle$. This mixing effect can therefore be simply taken into account by appropriate covalency factors in the expression of $\Delta\mathbf{g}(\mathbf{Fe^{2.5+}})$. For the sake of simplicity of the qualitative expressions, we will not write them explicitly for the moment.

Perhaps more importantly, and at the level of the mixed-valence pair (within the minority spin β orbitals), the same mixing and subsequent splitting of the "metal" and "ligand" levels, implies that a *complete* calculation of the $\Delta\mathbf{g}(\mathbf{Fe^{2.5+}})$-tensor involves further possible d−d transitions, first within the minority spin β levels (the occupied minority spin β ligand orbitals have now some minor iron content) and, to a lesser degree, within the majority spin levels. How can these contributions be taken into account? They are actually analogous to the contributions that make the ferric site tensor differ from $g_e \cdot \mathbf{Id}$. An actual calculation of $\Delta\mathbf{g}(\mathbf{Fe^{3+}})$ involves mainly transitions within the minority spin α set of molecular orbitals (following again the spin convention of Figure 3). By doing so, we obtain a nearly *isotropic* tensor $\Delta\mathbf{g}(\mathbf{Fe^{3+}}) \approx \Delta g(Fe^{3+}) \cdot \mathbf{Id}$ (with expectedly $\Delta g(Fe^{3+}) \approx 0.01-0.04$[46] as already given above). The many small contributions are roughly equally distributed among the g_{xx}, g_{yy}, and g_{zz} components of the tensor. By analogy, we can consequently model the additional contribution to $\Delta\mathbf{g}(\mathbf{Fe^{2.5+}})$ as $\Delta g(Fe^{2.5+}) \cdot \mathbf{Id}$. For the computation of the cluster **g**-tensor, these two isotropic contributions partly cancel each other because of the opposite signs of the spin projection coefficients K_{mv} and K_{3+} (see eq 2). The additional contribution to the total $\Delta\mathbf{g}$-tensor can be approximately expressed as

$$[2K_{mv}\Delta g(Fe^{2.5+}) + 2K_{3+}\Delta g(Fe^{3+})]\mathbf{Id} = \Delta g_{iso}(ox)\mathbf{Id} \quad (8)$$

As written, eq 8 serves in fact implicitly as a definition of the parameter $\Delta g_{iso}(ox)$. One can now calculate the (approximate) total $\Delta\mathbf{g}$-tensor in the (x,y,z) basis as the sum of eq 7 and eq 8:

$$\begin{cases} \Delta g_{xx} \approx (2K_{mv})\left(\frac{2\lambda}{4}\right)\frac{1}{\Delta\epsilon_{yz}} + \Delta g_{iso}(ox) \\ \Delta g_{yy} \approx (2K_{mv})\left(\frac{2\lambda}{4}\right)\frac{1}{\Delta\epsilon_{xz}} + \Delta g_{iso}(ox) \\ \Delta g_{zz} \approx (2K_{mv})\left(\frac{2\lambda}{4}\right)\frac{4}{\Delta\epsilon_{xy}} + \Delta g_{iso}(ox) \end{cases} \quad (9)$$

Because of the existence of a significant energy gap between the occupied $d_{x^2-y^2}$ and the set of the first bonding (empty) orbitals (~1.0 eV), relatively large compared to the relative energies within this set ($1/\Delta\epsilon_{xy} \approx 1/\Delta\epsilon_{xz} \approx 1/\Delta\epsilon_{yz}$), it can be easily verified that

(i) g_{zz} is indeed the largest of the three eigenvalues (hence $g_{zz} = g_1$) since d_{xy} is not high enough above d_{xz} and d_{yz} to compensate the roughly 4-fold increase of the numerator (again, the relative ordering of d_{xy}, d_{xz}, and d_{yz} is irrelevant to this first conclusion). The corresponding eigenvector $\mathbf{V}_1$ turns out to be the *z* axis, common perpendicular to the two pairs;

(ii) the calculated **g**-tensor is close to axiality. If some clear rhombicity appears, the two eigenvalues g_2 and g_3 should have their corresponding eigenvectors $\mathbf{V}_2$ and $\mathbf{V}_3$ aligned with the directions of the ferric and mixed-valence pairs (or vice versa). This point ii can serve as a complement to point i. If it is verified by itself, it yields the same information as point i since $(\mathbf{V}_1,\mathbf{V}_2,\mathbf{V}_3)$ forms a set of orthogonal axes.

Which eigenvector $\mathbf{V}_2$ or $\mathbf{V}_3$ corresponds to which axis **x** or **y** depends on the relative energetic ordering of the d_{xz} and d_{yz} spin−orbitals and the *D*'s (among other things). As an example, for $D_{xz} = D_{yz}$, exactly isotropic $\Delta g_{iso}(ox)$ and $\Delta\epsilon_{xz} < \Delta\epsilon_{yz}$ (cf. Figure 3), one would expect from eq 9 $g_{xx} = g_3$ and $g_{yy} = g_2$.

The result enunciated in point i has already been verified experimentally, for example, in a previous study of the nearly symmetric compound $(Et_4N)_2[Fe_4S_4(SCH_2Ph)_4]$. It holds true within a 20° dispersion of the angle values between $\mathbf{V}_1$ and the perpendicular axis to the two pairs.[10,12] Similar results can be observed for the $(Bu_4N)_2[Fe_4S_4(SPh)_4]$ compound. This is summarized in Table A of Appendix A (given as Supporting Information; see end of the article). Concerning the second point ii, and for the sake of clarity of the text, we report, also in Appendix A, the comparison of the cosines of the **Fe**−**Fe** directions in the crystallographic basis (**a**,**b**,**c***) of the eigenvectors $\mathbf{V}_2$ and $\mathbf{V}_3$ (associated with the eigenvalues g_2 and g_3)

of the **g**-tensors determined for the oxidized species of the same compound.[10] Notice that $\mathbf{V}_2$ is, as predicted above, systematically aligned with the direction of the ferric pair for centers of which the two pairs are identified[12] although the **g**-tensors are very axial (centers I−V).

The conclusion arrived at in point ii seems to be, in most cases, confirmed by the analysis of the experimental **g**-tensors. Consequently, these remarks serve as a useful guide for the identification of the mixed-valence and ferric pairs in $[4Fe-4S]^{3+}$ centers. More specifically, the comparison of $\mathbf{V}_1$ with perpendiculars to **Fe**−**Fe** directions seems to be robust, giving unambiguous information. To conclude, let us remark that there are many ways to get information from eq 9. It is possible, for example, to estimate values of $\Delta g_{iso}(ox)$ for the different centers and to relate them to ground spin states. This point is further discussed in Appendix B (Supporting Information).

(b) Lowering of the Symmetry. As mentioned above, the "rules of thumb" are *nearly* (but not exactly) verified, even for "symmetric" clusters: the eigenvectors of the actual measured **g**-tensors coincide nearly (center I is the exception) with the **Fe**−**Fe** pair directions or, for $\mathbf{V}_1$, the common perpendicular referred to as the **z** axis. The axes of the total **g**-tensor are essentially determined by those of the two local $\mathbf{g(Fe^{2.5+})}$-tensors (if there are corresponding distortions at the level of the ferric pair, they are expected to have little effect on the local ferric tensors and therefore on the total **g**-tensor). The distortion (lowering of the nuclear frame symmetry from the idealized C_{2v} used in our computations so far) could originate at the level of one of the two mixed-valence sites only or at both sites actually, then with or without symmetry relations between the two newly distorded sites. In the absence of more detailed information concerning the relaxation of the geometry upon oxidation, we propose to construct a mere *phenomelogical* model, leaving untouched the occupied delocalized $d_{x^2-y^2}{}^{+}$ orbital and allowing mixing within the $\{d_{xy}{}^{+}, d_{xz}{}^{+}, d_{yz}{}^{+}\}$ set to occur. As it turns out, very small mixings of the molecular orbitals are indeed sufficient to result in angular values as high as 20°. This is presented in details as Supporting Information in Appendix C.

We dealt so far in the previous paragraph with geometrical distortions only, without chemical change. However, another way of breaking the idealized C_{2v} symmetry consists in changing the immediate chemical environment of the cluster. Such is actually the case of the $(Et_4N)_2[Fe_4S_4(SC_6H_4\text{-}o\text{-}OH)_4]$ compound studied in this paper, presenting an extra (fifth) coordination at the level of iron 1. If the unique iron site Fe_1 belongs to the ferric pair, the **g**-tensor should follow very much the above "rule of thumb" regarding the direction of the largest g-value because of the relative insensivity of the spherical d^5 configuration to its surrounding. If however the unique iron site belongs to the mixed-valence pair, the symmetry between the two ions is destroyed, leading perhaps to the *localization* of the extra electron on one of the two iron atoms of the pair, depending on the strength of the perturbation. The resulting system of eigenvectors could then become unpredictable. We suspect however that the perturbation induced by the pentacoordination on Fe_1 is small. In effect, the $Fe_1-O_1(H)$ bond (∼2.3 Å) is a weak coordination bond, much weaker than Fe−O bonds with unprotonated oxygens which, generally, have lengths around 1.9−2.1 Å.

(3) g-Tensor Model for the $[4Fe-4S]^{+}$ State. After the relatively simple treatment involved for the computation of the **g**-tensor of $[4Fe-4S]^{3+}$ clusters, we want to consider now the case of a "symmetric" $[4Fe-4S]^{+}$ cluster (with two equivalent iron atoms in the mixed-valence pair, here again along **x**, and in the ferrous pair, along **y**). A schematic orbital energy diagram is shown in Figure 4 (here for the configuration OC2;[30,48] see below). We observe first that the delocalized mixed-valence pair can be treated as for the $[4Fe-4S]^{3+}$ center (cf. eq 7 and the first part of eq 9 for its expression).

The difference with the previous treatment on the "oxidized" cluster lies now at the level of the *ferrous* pair where we find two minority spin α-electrons rather than none as for the ferric pair of $[4Fe-4S]^{3+}$. One electron energy level occupies a molecular orbital whose main character is $d_{x^2-y^2}{}^{+}$ as for the mixed-valence pair (implying transitions within the + phased MO's) whereas the second one can occupy either a $d_{z^2}{}^{-}$ orbital, defining configuration OC1, or a $d_{xz}{}^{-}$ orbital, resulting in configuration OC2. Notice that both levels present the same "−" phase and are lying very close in energy.[30,48] The existence of two electronic configurations OC1 and OC2 leads of course to a doubling of the number of reduced centers potentially observable.

Apart from the promotion of the electron in the $d_{x^2-y^2}{}^{+}$ into the three contributing empty orbitals ($d_{xy}{}^{+}$, $d_{xz}{}^{+}$, $d_{yz}{}^{+}$), the most substantial contribution to the site ferrous tensor comes certainly from the promotion of the second higher electron into the next quasi-degenerate orbital (involving $d_{z^2}{}^{-}$ and $d_{xz}{}^{-}$). Both OC1 and OC2 involves the same matrix elements in the calculation of this last contribution to the $\Delta\mathbf{g(Fe^{2+})}$-tensor. Some care has to be taken of these matrix elements however. For example, there is possibly mixing, within the B_2 set, of the two orbitals $d_{z^2}{}^{-}$ and $d_{x^2-y^2}{}^{-}$ (see the resulting character of this $14B_2$ orbital in Figure 3 of ref 29 as well as Figure 8). To avoid writting cumbersome expressions below, we will proceed first in an analysis of OC1 and OC2 as simple as that presented for oxidized clusters (with "pure" $d_{z^2}{}^{-}$ and $d_{xz}{}^{-}$ orbitals) and will, only at the end, *modulate* the results obtained by the existence of these additional components.

To proceed therefore further, we now want to distinguish between the two configurations OC1 and OC2, without introducing covalency factors in order to simplify the expressions below.

(a) Case of OC1 ($\mathbf{d_{z^2}{}^{-}}$ below $\mathbf{d_{xz}{}^{-}}$). The explicit calculation of the contribution of each ferrous ion (marked by upper indices "2+" in ϵ^{2+}), within our simple assumptions, is made of two parts, as exemplified in eq 10:

$$K_{2+}\times\left(\frac{2\lambda}{4}\right)\times\left\{\begin{pmatrix}\frac{1}{\epsilon^{2+}_{yz}-\epsilon^{2+}_{x^2-y^2}} & 0 & 0\\ 0 & \frac{1}{\epsilon^{2+}_{xz}-\epsilon^{2+}_{x^2-y^2}} & 0\\ 0 & 0 & \frac{4}{\epsilon^{2+}_{xy}-\epsilon^{2+}_{x^2-y^2}}\end{pmatrix}+\begin{pmatrix}\frac{3}{\epsilon^{2+}_{yz}-\epsilon^{2+}_{z^2}} & 0 & 0\\ 0 & \frac{3}{\epsilon^{2+}_{xz}-\epsilon^{2+}_{z^2}} & 0\\ 0 & 0 & 0\end{pmatrix}\right\} \quad (10)$$

The first contribution calculated for the ferrous site will partially *compensate* the contributions coming from the mixed-valence pair (K_{mv} and K_{2+} have opposite signs: cf. eq 7 and/or eq 9). Recall also again that, onto passing from one pair to the other, the "*x*" and "*y*" subscripts are interchanged as far as the description of the characters of the orbitals is concerned (see

(48) Noodleman, L. *Inorg. Chem.* **1991**, *30*, 256.

Figure 4). We therefore have the following approximate correspondence:

$$\begin{cases} \varepsilon^{mv}_{xy}-\varepsilon^{mv}_{x^2-y^2} \approx \varepsilon^{2+}_{xy}-\varepsilon^{2+}_{x^2-y^2} & \Rightarrow \quad \Delta\varepsilon_{xy} \\ \varepsilon^{mv}_{xz}-\varepsilon^{mv}_{x^2-y^2} \approx \varepsilon^{2+}_{yz}-\varepsilon^{2+}_{x^2-y^2} & \Rightarrow \quad \Delta\varepsilon_{xz} \\ \varepsilon^{mv}_{yz}-\varepsilon^{mv}_{x^2-y^2} \approx \varepsilon^{2+}_{xz}-\varepsilon^{2+}_{x^2-y^2} & \Rightarrow \quad \Delta\varepsilon_{yz} \end{cases} \tag{11}$$

Introducing here again the parameter $\Delta g_{iso}(rd) = [2K_{mv}\Delta g(Fe^{2.5+}) + 2K_{2+}\Delta g(Fe^{2+})]$, in close analogy to the analysis presented above for $[4Fe-4S]^{3+}$, we have finally for the total **g(OC1)**-tensor:

$$\begin{cases} \Delta g_{xx} \approx \left(\frac{2\lambda}{4}\right)\times\left[\frac{2K_{mv}}{\Delta\varepsilon_{yz}}+\frac{2K_{2+}}{\Delta\varepsilon_{xz}}\right]+\left(\frac{2\lambda}{4}\right)\times\left[\frac{6K_{2+}}{\varepsilon^{2+}_{yz}-\varepsilon^{2+}_{z^2}}\right]+\Delta g_{iso}(rd) & \Rightarrow \quad g_2 \\ \Delta g_{yy} \approx \left(\frac{2\lambda}{4}\right)\times\left[\frac{2K_{mv}}{\Delta\varepsilon_{xz}}+\frac{2K_{2+}}{\Delta\varepsilon_{yz}}\right]+\left(\frac{2\lambda}{4}\right)\times\left[\frac{6K_{2+}}{\varepsilon^{2+}_{xz}-\varepsilon^{2+}_{z^2}}\right]+\Delta g_{iso}(rd) & \Rightarrow \quad g_3 \\ \Delta g_{zz} \approx \left(\frac{2\lambda}{4}\right)\times\left[\frac{4}{\Delta\varepsilon_{xy}}\right] +\Delta g_{iso}(rd) & \Rightarrow \quad g_1 \end{cases} \tag{12}$$

The first contribution in eqs 10 and 12 is nearly axial (as directly verifiable for the **g**-tensors of the $[4Fe-4S]^{3+}$ centers). Since $2K_{mv} + 2K_{2+} = 1$ and, from the predicted and observed axiality of the $[4Fe-4S]^{3+}$ **g**-tensor, $1/\Delta\epsilon_{yz} \approx 1/\Delta\epsilon_{xz} \approx 1/\Delta\epsilon_{xy} \approx 1/\Delta\epsilon$, the first braket terms in Δg_{xx}, Δg_{yy} and that of Δg_{zz} yield a roughly axial contribution to the Δ**g**-tensor of the form $\sim(\lambda/2\Delta\epsilon, \lambda/2\Delta\epsilon, 2\lambda/\Delta\epsilon)$. When compared to the case of a $[4Fe-4S]^{3+}$ center, the partial compensation discussed above contributes already to the lowering of the value taken by g_{av} and to the fact that g_{zz} will be somewhat smaller than in $[4Fe-4S]^{3+}$. Among the second terms contributing to the **xx** and **yy** components, that of **yy** is expected to be the largest because of the quasi-degeneracy of the d_{xz}^- and $d_{z^2}^-$ molecular orbitals.

The system of equations eq 12 is interesting, at first qualitatively, for the identification of g_1, g_2, and g_3. When we compare these expressions with those obtained for a $[4Fe-4S]^{3+}$ center, we now notice the presence of negative contributions (because $K_{2+} < 0$). We arrive at the following conclusions for OC1:

(i) The largest eigenvalue g_1 is expected to have its eigenvector $\mathbf{V}_1$ aligned with the **z** axis (as in the case of $[4Fe-4S]^{3+}$). It is also expected to be somewhat smaller than in the case of oxidized $[4Fe-4S]^{3+}$ clusters.

(ii) A large rhombicity (g_{yy} being identified as g_3, the smallest eigenvalue of the **g**-tensor) is introduced by the quasi-degeneracy of the d_{xz}^- and $d_{z^2}^-$ orbitals.

(iii) The eigenvector $\mathbf{V}_3$ (associated with g_3) is expected to be aligned along the direction of the *ferrous* pair whereas $\mathbf{V}_2$ would be directed along **x**, that is along the mixed-valence pair (this can be tested by considering measured **g**-tensors, where the location of the pair is known: see below).

(b) Case of OC2 (d_{xz}^- below $d_{z^2}^-$). The expressions involved are a little more complicated than in the case of OC1 (especially for g_3, whose experimental value is expected to be greatly variable anyway). For each ferrous site, we now have eq 13:

$$K_{2+}\left(\frac{2\lambda}{4}\right)\times\left\{\begin{pmatrix} \frac{1}{\varepsilon^{2+}_{yz}-\varepsilon^{2+}_{x^2-y^2}} & 0 & 0 \\ 0 & 0 & 0 \\ 0 & 0 & \frac{4}{\varepsilon^{2+}_{xy}-\varepsilon^{2+}_{x^2-y^2}} \end{pmatrix} + \begin{pmatrix} \frac{3}{\varepsilon^{2+}_{xy}-\varepsilon^{2+}_{xz}} & 0 & 0 \\ 0 & \frac{3}{\varepsilon^{2+}_{z^2}-\varepsilon^{2+}_{xz}} & 0 \\ 0 & 0 & \frac{1}{\varepsilon^{2+}_{yz}-\varepsilon^{2+}_{xz}} \end{pmatrix}\right\} \tag{13}$$

Through the use of an artifice—addition/subtraction—in the expression of g_{yy} so as to keep the same forms of its first part as in OC1, the expression of the full **g(OC2)**-tensor becomes therefore that in eq 14. One significant difference, when comparing eq 14 to eq 12 is the appearance of a negative contribution in Δg_{zz} (in contrast to OC1). It could therefore happen that the **g(OC2)**-tensor becomes closer to axiality in some cases (with $g_\perp > g_{||}$) or even inverts the ordering of the eigenvalues g_{xx} and g_{zz} (g_1 and g_2) in which case $\mathbf{V}_1$ would possibly become aligned with the direction of the mixed-valence pair rather than being perpendicular to that pair ($\mathbf{V}_3$ is expected to remain parallel to the ferrous pair anyway).

(c) Discussion. A first test of our conclusions on the $[4Fe-4S]^+$ state consists of comparing our predictions (see points i−iii above, defined for OC1) with the eigenvectors of experimental diagonalized **g**-tensors of synthetic model compounds in their reduced states (see for example the case of center A in $[Fe_4S_4(SPh)_4]^{3-}$ or centers I_R and II_R in $[Fe_4S_4(SCH_2Ph)_4]^{3-}$ in Appendix D; see Supporting Information). It is there shown that, when $\mathbf{V}_2$ and $\mathbf{V}_3$ are aligned with **Fe**−**Fe** directions, points i and iii yield compatible results, as for center A in $[Fe_4S_4(SPh)_4]^{3-}$ or center II_R in $[Fe_4S_4(SCH_2Ph)_4]^{3-}$).

These results are potentially very interesting for the interpretation of the **g**-tensors in the proteins. We want to point out that the most important predictions of our theoretical model are those pertaining to the principal directions of the **g**-tensors. However, until quite recently, no study could be invoked to substantiate our propositions, apart from those conducted on membrane proteins because of their orientation in the membrane. This is the case of the Photosystem I (PS I) system, of which the structural organization of the three reduced [4Fe−4S] iron−sulfur centers had been already inferred from EPR studies, by simulating powder spectra of the coupled state (F_A^-, F_B^-) on oriented thylakoid membranes.[49] Very recently, new EPR study by Stehlik, Kamlowski et al. on the iron−sulfur centers F_A and F_B of PS I has been completed.[50,51] Their complete **g**-tensors, i.e., including the orientation of the corresponding principal axes

$$\begin{cases} \Delta g_{xx} \approx \left(\frac{2\lambda}{4}\right)\times\left[\frac{2K_{mv}}{\Delta\varepsilon_{yz}}+\frac{2K_{2+}}{\Delta\varepsilon_{xz}}\right]+\left(\frac{2\lambda}{4}\right)\times\left[\frac{2K_{2+}}{\varepsilon^{2+}_{xy}-\varepsilon^{2+}_{xz}}\right] +\Delta g_{iso}(rd) & \Rightarrow \quad g_2 \\ \Delta g_{yy} \approx \left(\frac{2\lambda}{4}\right)\times\left[\frac{2K_{mv}}{\Delta\varepsilon_{xz}}+\frac{2K_{2+}}{\Delta\varepsilon_{yz}}\right]+\left(\frac{2\lambda}{4}\right)\times\left[2K_{2+}\left(\frac{3}{\varepsilon^{2+}_{z^2}-\varepsilon^{2+}_{xz}}-\frac{1}{\Delta\varepsilon_{xz}}\right)\right]+\Delta g_{iso}(rd) & \Rightarrow \quad g_3 \\ \Delta g_{zz} \approx \left(\frac{2\lambda}{4}\right)\times\left[\frac{4}{\Delta\varepsilon_{xy}}\right] +\left(\frac{2\lambda}{4}\right)\times\left[\frac{2K_{2+}}{\varepsilon^{2+}_{yz}-\varepsilon^{2+}_{xz}}\right] +\Delta g_{iso}(rd) & \Rightarrow \quad g_1 \end{cases} \tag{14}$$

with respect to the clusters, have been determined on single crystals of PS I from a cyanobacterium, *Synechococcus elongatus*. As it turns out, they found V_1 perpendicular to both Fe−Fe vectors of the ferrous and mixed-valence pairs (a conclusion differing somewhat from that of Guigliarelli et al.). On the other hand, $\mathbf{V}_2/\mathbf{V}_3$ were found collinear to these same Fe−Fe pairs (although permuted when compared to our present predictions).

To conclude, although for nearly symmetric compounds, we would expect $\mathbf{V}_2$ and $\mathbf{V}_3$ to be aligned with the directions of the pairs of iron atoms, this can be less trivially verified at the empirical level because the ferrous ion is more sensitive to its immediate environment than the ferric ion. This sensitivity could possibly break the kind of "mirror symmetry" we imposed so far on the two ferrous ions. We must also point out that these rules may completely fail for less symmetric $[4Fe-4S]^+$ centers (as in the present paper, where the compound studied has an extra-coordination on Fe_1). If the unique Fe_1 belongs to the mixed-valence pair, we do not expect that this will invalidate the above "rule of thumb" unless the pair becomes localized. However, if the Fe_1 site belongs to the ferrous pair, our rule may not applied, and the axes of the **g**-tensor may have no relation to Fe−Fe directions. Moreover, the configuration OC2 (in contrast to OC1) could possibly exhibit an exchange of eigenvectors ($\mathbf{V}_1$ and $\mathbf{V}_2$) in addition to mixing of $\mathbf{V}_3 = \mathbf{V}_{yy}$ with $\mathbf{V}_{zz} = \mathbf{V}_1$ or $\mathbf{V}_2$ ($\mathbf{V}_1$ for OC1).

(2) Proposed Assignments for the Different Centers. Center 1. Since center 1 has $g_{av} > g_e$, it is clearly a $[4Fe-4S]^{3+}$ center. It has a somewhat more rhombic tensor than often found in oxidized HiPIP proteins or synthetic analogues. The principal direction $\mathbf{V}_1$ is 3° away from $(\mathbf{Fe_1}-\mathbf{Fe_2}) \times (\mathbf{Fe_3}-\mathbf{Fe_4})$ (common perpendicular to these two **Fe**−**Fe** directions) (cf. Table 2). Its mixed-valence pair is therefore localized on either Fe_1-Fe_2 or on Fe_3-Fe_4. The eigenvectors $\mathbf{V}_2$ and $\mathbf{V}_3$ are close to the directions of $\mathbf{Fe_1}-\mathbf{Fe_2}$ and $\mathbf{Fe_3}-\mathbf{Fe_4}$ respectively, thus confirming the information obtained from the consideration of $\mathbf{V}_1$ alone.

Centers 2 and 3. With $g_{av} > g_e$, both are $[4Fe-4S]^{3+}$ centers. The **g**-tensors are nearly axial and typical of oxidized HiPIP proteins or synthetic analogues previously studied in single crystals.[10] Their principal directions $\mathbf{V}_1$ are not far from $(\mathbf{Fe_1}-\mathbf{Fe_4}) \times (\mathbf{Fe_2}-\mathbf{Fe_3})$ (20° and 3°, respectively) as observed for symmetric compounds (see Table A of Appendix A). The eigenvector $\mathbf{V}_2$ of center 3 is 8° away from $\mathbf{Fe_2}-\mathbf{Fe_3}$ (and $\mathbf{V}_3$ 9° away from $\mathbf{Fe_2}-\mathbf{Fe_3}$) further confirming this assignment. This suggests to us that these two centers are complementary, i.e., one has its mixed-valence pair localized on Fe_1-Fe_4 and the other has it on Fe_2-Fe_3, as already discussed.[10] Moreover, in center 2, Fe_1 could be part of the mixed-valence pair whereas its presence within a ferric pair (as would be the case for center 3) would have no visible effect. We can see here that the presence of Fe_1 in a mixed-valence pair, as probably true for center 2, does not apparently invalidate our "rule of thumb" i, as anticipated above.

The principal values of these three first tensors, as well as their estimated $\Delta g_{iso}(ox)$ parameters (see Table 3) make these three oxidized centers somewhat analogous to the "lateral" centers in the "symmetric" compound (centers I, II, and V); see Table B of Appendix B. We notice moreover that, for centers 1 and 2, the angles of $\mathbf{V}_2$ and $\mathbf{V}_3$ with **x** and **y** are large (∼30−42°). This seems to be also the rule for the reduced centers 4−7. This observation may be correlated with the perturbation introduced by the extra (fifth) coordination at the level of Fe_1 (see Table A; center I presents the same type of behavior and is known to have a distorted geometry relative to that of the 2+ compound).

Table 3. Values of $\Delta g_{iso}(ox)$ and of the Ratios $\Delta g_1/\Delta g_2$ and $\Delta g_1/\Delta g_3$ (See Main Text) for the Three "Oxidized" Centers in the "Asymmetric" Compound

	$\Delta g_{iso}(ox)$	$\Delta g_1/\Delta g_2$	$\Delta g_1/\Delta g_3$	$(g_2 - g_3)/(g_1 - g_3)$
center 1	−0.04	∼5	∼(−6)	0.31
center 2	−0.02	∼8	∼13	0.04
center 3	−0.03	∼8	∼(−43)	0.15

Center 4. This center is very peculiar since it has a g_{av} value equal to g_e, and it is therefore difficult to assign it firmly to $[4Fe-4S]^{3+}$ or $[4Fe-4S]^+$. Its **g**-tensor is somewhat rhombic as generally found for $[4Fe-4S]^+$ centers and it resembles in some way center II_R of the "symmetric" compound[10] $[Fe_4S_4(SCH_2Ph)_4]^{3-}$ (notice a value g_{av} of 1.992 and the high g_1 value of 2.087 for this last center). Moreover, since we do not know any $[4Fe-4S]^{3+}$ center with a g_3 value as low as 1.937, we assign to it a $[4Fe-4S]^+$ state. The smallest angle between the principal direction $\mathbf{V}_1$ and $(\mathbf{Fe_1}-\mathbf{Fe_3}) \times (\mathbf{Fe_2}-\mathbf{Fe_4})$ is 32°. Thus, its mixed-valence pair could be either on Fe_1-Fe_3 or on Fe_2-Fe_4. $\mathbf{V}_3$ makes here an angle of 60° and 34°, respectively, with these **Fe**−**Fe** directions whereas $\mathbf{V}_2$ (aligned, according to theory, with the mixed-valence pair in reduced centers) has an angle of 37° and 68°, respectively, with the same **Fe**−**Fe** directions. We could therefore assign Fe_1-Fe_3 as the mixed-valence pair of this peculiar center, but this is rather tentative (notice that Fe_1 would then belong to the mixed-valence pair). Based on the discussion above, center 4 would be in an OC1 electronic state.

Incidentally, we notice a relatively good correlation between $(\mathbf{V}_1,\mathbf{V}_2)$ and $(\mathbf{Fe_2}-\mathbf{Fe_3}, \mathbf{Fe_1}-\mathbf{Fe_4})$. Moreover, $\mathbf{V}_1$ is (nearly) parallel to the common perpendicular of these two Fe−Fe directions. This would, however, correspond to an exchange of the g_1 and g_3 eigenvalues, an exchange whose origin could not possibly be understood with the present model.

Center 5. Its g_{av} value indicates that it is a $[4Fe-4S]^+$ center. However, its **g**-tensor differs from all cases presented before for this state in that it is close to axiality, but with $g_\perp > g_\parallel$. This is compatible with a possible property of the configuration OC2, namely a relatively low $g_1 \approx g_2$ value, whereas OC1 yields rather *rhombic* **g**-tensors. Since $\mathbf{V}_1$ is close to $(\mathbf{Fe_1}-\mathbf{Fe_3}) \times (\mathbf{Fe_2}-\mathbf{Fe_4})$, its mixed-valence pair will be on either of these two pairs. $\mathbf{V}_3$ is 30° away from $\mathbf{Fe_1}-\mathbf{Fe_3}$ (61° away from $\mathbf{Fe_2}-\mathbf{Fe_4}$) whereas $\mathbf{V}_2$ is found at 31° of $\mathbf{Fe_2}-\mathbf{Fe_4}$ (60° of $\mathbf{Fe_1}-\mathbf{Fe_3}$), thus identifying with good probability Fe_2-Fe_4 as being the mixed-valence pair. As far as the locations of the mixed-valence pairs are concerned, centers 4 and 5 could be said to be complementary although they might have different electronic structures.

Centers 6, 6′, and 6″. The common g_{av} value identify 6, 6′, and 6″ as $[4Fe-4S]^+$ centers. Their **g**-tensors are very similar and their principal directions differ only by few degrees. This suggests to us that they are different varieties of the same center type and, consequently, that they have their mixed-valence pair certainly localized on the same two iron atoms. In our view they represent a new example of the situation already observed in the $(Et_4N)_2[Fe_4S_4(SCH_2Ph)_4]$ crystals[10] (and especially the fully deuterated ones), where centers III and III′ were very similar and where the centers I and II each exhibit satellite lines corresponding to several varieties nearly identical with them. We think therefore that, exactly as in this previous study, these three reduced species 6, 6′, and 6″ must be trapped in the vicinity of a structural defect in the crystal (a dislocation or a stacking

(49) Guigliarelli, B.; Guillausier, J.; More, C.; Sétif, P.; Bottin, H.; Bertrand, P. *J. Biol. Chem.* **1993**, *268*, 900−908.
(50) Kamlowski, A.; Est, A. v. d.; Fromme, P.; Stehlik, D. *Biochim. Biophys. Acta* **1997**, in press.
(51) Kamlowski, A.; Est, A. v. d.; Fromme, P.; Krauss, N.; Schubert, W.-D.; Klukas, O.; Stehlik, D. *Biochim. Biophys. Acta* **1997**, in press.

fault) although at different sites around it, the proximity of this common defect inducing slight specific geometric disturbances leading to slightly different **g**-tensors. Coming to their nearly common direction $\mathbf{V}_1$, we find that it is close (between 2° and 8°) to (**Fe$_1$**−**Fe$_4$**) × (**Fe$_2$**−**Fe$_3$**) (only data for center 6 are reported in Table 2). Moreover, **Fe$_1$**−**Fe$_4$** is the closest direction (between 30° and 35°) to $\mathbf{V}_3$ while **Fe$_2$**−**Fe$_3$** is the closest one (between 28° and 35°) to $\mathbf{V}_2$. The mixed-valence pair is most probably Fe_2-Fe_3. The rhombic character of these tensors, as well as rather large g_1 values, suggest that the ferrous pair is of the OC1-type.

Center 7. It has a g_{av} value typical of the reduced state of ferredoxins. The anisotropy of **g** is also typical of this ferredoxin reduced state, but **g** has the peculiarity to be nearly axial with $g_{\|} > g_{\perp}$. $\mathbf{V}_1$ is close to (**Fe$_1$**−**Fe$_2$**) × (**Fe$_3$**−**Fe$_4$**). Its near axiality makes it difficult to extract further information from the consideration of $\mathbf{V}_2$ or $\mathbf{V}_3$. We suspect that center 7 has its mixed-valence pair on Fe_3-Fe_4 (let us still notice that $\mathbf{V}_3$ lies at 39° of **Fe$_1$**−**Fe$_2$** whereas $\mathbf{V}_2$ is at 37° of **Fe$_3$**−**Fe$_4$**, thus "confirming" this assignment). This suggests that Fe_1 is a ferrous site. This does not invalidate the "rule of thumb" based on g_1.

Centers 8 and 9. These reduced centers are alike and form a separate group. Their **g**-tensors are rhombic with rather similar anisotropies. The g_1 values (1.98 and 1.97, respectively) are significantly lower than g_e whereas the g_3 values are the smallest of the whole set of data (1.82 and 1.80, respectively, discussed below). We have found no obvious correlation beween $\mathbf{V}_1$ and common perpendiculars to the pairs of Fe−Fe bonds: the "rule of thumb" is not verified at all. For this situation, it does not make much sense to rely on the use of $\mathbf{V}_2$ or $\mathbf{V}_3$. These eigenvectors are close, for both centers, to **Fe**−**Fe** directions, but these have Fe_1 in common for center 8 and Fe_4 in common for center 9.

The use of ENDOR for center 8 (see the following companion paper in Part 2) identifies Fe_2-Fe_3 as the mixed-valence pair. But we already identified Fe_2-Fe_3 as the mixed-valence pair in center 6. The resolution of this apparent contradiction lies in the fact that this center 8, from the consideration that g_1 is lower than g_e, adopts most probably the OC2 electronic configuration (despite its strong rhombicity), in contrast to center 6 which has an OC1 configuration. It is then puzzling to compare the directions (known through ENDOR) of the two pairs with the Fe−Fe directions predicted by our simple analytical model. The vector $\mathbf{V}_1$ lies at 47° of (**Fe$_2$**−**Fe$_3$**) × (**Fe$_1$**−**Fe$_4$**), $\mathbf{V}_2$ at 73° of **Fe$_2$**−**Fe$_3$** and $\mathbf{V}_3$ at 71° of **Fe**$_1$−**Fe**$_4$. This is surely related to the fact that the mixed-valence pair, as indirectly observed by ENDOR, is *localized* rather than delocalized as in our model (see conclusions of Part 2). We still notice that $\mathbf{V}_2$ lies at 30° of (**Fe$_1$**−**Fe$_2$**) × (**Fe$_3$**−**Fe$_4$**), $\mathbf{V}_1$ at 26° of **Fe$_3$**−**Fe$_4$**, and $\mathbf{V}_3$ at 15° of **Fe$_1$**−**Fe$_2$** again to make us cautious about any "good" agreement.

Consequently, the Fe_1 being part of the ferrous pair in both center 6 and center 8, this would illustrate the dramatic effect of a change in electronic configuration upon the **g**-tensors (accompanied by a nearby crystalline defect in the latter case, as demonstrated in Part 2). It is interesting to notice that rather low g_3 values ($\leq$1.80) have been observed for biological systems departing from the "classical" 4Fe cluster ligated to four cysteines. A first example is provided by the 4Fe cluster ferredoxin from *P. furiosus*[3] (with three Cys and one Asp ligation sites[52]). For that system (when anaerobically isolated), the reduced cluster presents a spin mixture of $S = {}^1/_2$ (20%) and $S = {}^3/_2$ (80%) ground states, the first being characterized by rhombic resonance at $g_1 = 2.10$, $g_2 = 1.87$, and $g_3 = 1.80$. Several substrate bound states of aconitase yield similar *g*-factor patterns characterized by $2.01 \leq g_1 \leq 2.04$, $1.85 \leq g_2 \leq 1.87$ and $1.77 \leq g_3 \leq 1.79$ (*trans*-aconitate substrate[53]). Moreover, Mössbauer studies performed on substrate-bound aconitase show clearly a asymmetry within the ferrous pair, with average ^{57}Fe hyperfine parameters +31 MHz (binding site) and +15 MHz.[54] The non-Cys ligand (aspartic acid or hydroxyl/water) may thus lead to possible cubane distortions and breaking of our "rule of thumbs" elaborated for "symmetric" systems.

Table 4. Classification of the "Oxidized" and "Reduced" Centers in the "Asymmetric" Compound

center	redox state	mv pair
1	ox	1 & 2 or 3 & 4
2	ox	1 & 4 or 2 & 3
3	ox	2 & 3 or 1 & 4
4	rd	1 & 3
5	rd	2 & 4
6	rd	2 & 3
7	rd	3 & 4
8	rd	2 & 3[a]
9	rd	?

[a] As inferred from proton ENDOR spectroscopy.

About center 9, it can be said that (i) it closely resembles center 8 in its angular dependencies, (ii) it has essentially the same eigenvalues, (iii) it presents the same breaking of the "rule of thumb" and the same "coincidences" at the level of $\mathbf{V}_2$ and $\mathbf{V}_3$, and (iv) it has most probably the same electronic configuration. It is striking that the **g**-tensors of centers 8 and 9 are seemingly related through a mirror plane containing **Fe$_2$**−**Fe$_3$** while perpendicular to **Fe$_1$**−**Fe$_4$**. The kind of mirror-symmetry relating the **g**-tensors of centers 8 and 9 is also puzzling since Fe_1 and Fe_4 are both ferrous in center 8. Were the (localized) mixed-valence pair located on these two iron atoms, one could have envisaged an exchange of the ferric and ferrous ions explaining the symmetry. Without "rules of thumb", nothing more can be said: the question would have to be solved (if feasible) by ENDOR spectroscopy.

In concluding this review of the assignments we propose for these different centers, we want to point out that the collection of values found here for the reduced centers 4−9 even presents a wider diversity than the one found in the proteins. We suppose that this large diversity is basically generated, here again, by the diverse possibilities to place the mixed-valence pair on two iron atoms, but that it is here modulated by the effects carried by the inequivalence between iron atoms.

Conclusions

The assignments previously proposed for the different centers studied here are listed in Table 4. They comprise the most plausible and reasonable set of assignments that we are able to propose yet for the interpretation of the present data. Nevertheless, we are well aware of the tentative value of some of these assignments. In effect, the **g**-tensors which constitute most often the first element of knowledge on paramagnetic iron−sulfur states are global and relatively opaque observables which do not generally give detailed information about the electronic structure of the species, except if symmetry considerations can be used. Thus, by starting from what we know for quasi-symmetric models of the structure (represented in Figures 3 and 4), we have developed qualitative as well as semiquantitative arguments for the rationalization of the whole set of data,

(52) Calzolai, L.; Gorst, C. M.; Zhao, Z.-H.; Teng, Q.; Adams, M. W. W.; LaMar, G. N. *Biochemistry* **1995**, *34*, 11373−11384.

(53) Telser, J.; Emptage, M. H.; Merkle, H.; Kennedy, M. C.; Beinert, H.; Hoffman, B. M. *J. Biol. Chem.* **1986**, *261*, 4840−4846.

(54) Kent, T. A.; Emptage, M. H.; Merkle, H.; Kennedy, M. C.; Beinert, H.; Münck, E. *J. Biol. Chem.* **1985**, *260*, 6871−6881.

summarized in Table 1. The explicit calculation of the total **g**-tensors relied on angular overlap approximations as far as the construction of a proper energy level diagram is concerned. This allowed us to derive a "rule of thumb" (based on g_1 and $\mathbf{V}_1$), further completed by an analysis of $\mathbf{V}_2$ and $\mathbf{V}_3$, thus leading to a possible identification of the pairs. This approach puts in evidence the marked difference about what we can say on one hand for the $[4Fe-4S]^{3+}$ states and, on the other hand, for the $[4Fe-4S]^{+}$ states.

For the $[4Fe-4S]^{3+}$ states, we confirm the suggestion acquired in previous results,[10,55] that the direction $\mathbf{V}_1$ along the largest principal *g*-value, g_1, is a reliable guide that allows the determination of the location of the mixed-valence pair.

The situation is less clear for the $[4Fe-4S]^{+}$ states; centers 4, 5, and 7 have indeed unusual **g**-tensors. Moreover, we have to take into account the doubling of possible reduced centers due to the existence of two quasi-degenerate electronic configurations, called OC1 and OC2.[30,48] Furthermore, there is a peculiar difficulty for these states in *asymmetrical* structures, which is due to the greater sensitivity of the ferrous ions to the details of their immediate surrounding. Consequently, $\mathbf{V}_1$ is a somewhat less certain guide in $[4Fe-4S]^{+}$ for identifying the disposition of the mixed-valence pair. Since we consider the perturbation by the fifth ligand of Fe_1 as moderate at the chemical level, we have continued to use our model with caution, when Fe_1 belongs to the mixed-valence pair, taking into account the asymmetry that it introduces. However, the examples of centers 8 and 9 show that if the ferrous pair is not symmetric, nearly any **g**-tensor can then be obtained and that correlations between axes and directions of pairs of iron atoms will be lost. This makes the identification of the positions of the ferrous ions and of the mixed-valence pair quasi impossible for those two last centers. Another clear limit of the discussion and rationalization that we have followed here is that there can be other sources of possible inequivalence of the iron atoms playing a role simultaneously with the ones considered here. This would complicate the problem and they were, of course, neglected here. Ultimately, then, a first but limited knowledge of the different centers studied here was obtained, and the only way to go further and put their identifications on a firm ground is to measure hyperfine interaction tensors by ENDOR (or equivalently pulsed EPR) methods.

(55) Crozet, M. Thesis, University Joseph Fourier, Grenoble I, 1995.

Acknowledgment. We thank Mr Gérard Desfonds for his high technical competence and his kind help in several aspects of the practical realization of this work. We also thank professor Eckard Münck for helpful discussions, careful proof reading of the manuscript, and constructive suggestions for improving it (especially in the discussion of Figures 3−5) during his stay in Grenoble (June 1996), as well as Dr. Louis Noodleman for appreciated critical remarks on the theoretical section of this paper.

Supporting Information Available: Appendices A−D, as well as the corresponding Tables A−D (11 pages). See any masthead page for ordering and Internet access instructions.

JA963349O